Turun yliopisto
University of Turku

LANTHANIDE DOPED $NaYF_4$ UP-CONVERSION LUMINESCENCE MATERIALS

Tero Laihinen

TURUN YLIOPISTON JULKAISUJA – ANNALES UNIVERSITATIS TURKUENSIS
Sarja - ser. AI osa - tom. 550 | Astronomica - Chemica - Physica - Mathematica | Turku 2016

University of Turku

Faculty of Mathematics and Natural Sciences
Department of Chemistry
Laboratory of Materials Chemistry and Chemical Analysis
Doctoral Programme in Physical and Chemical Sciences

Supervised by

Docent Mika Lastusaari
Department of Chemistry
University of Turku
FI-20014 Turku, Finland

Dr. Techn. Jorma Hölsä
Department of Physics
University of the Free State
ZA-9300 Bloemfontein, South Africa

Custos

Docent Mika Lastusaari
Department of Chemistry
University of Turku
FI-20014 Turku, Finland

Reviewed by

Professor Maarit Karppinen
Department of Chemistry
School of Chemical Technology
Aalto University
P.O. Box 16100, FI-00076 Aalto, Finland

Dr. Sebastian Vielhauer
Institute of Physics
University of Tartu
W. Ostwaldi 1, EE-50411 Tartu, Estonia

Opponent

Dr hab. Dariusz Hreniak
Institute of Low Temperature and Structure Research
Polish Academy of Sciences
ul. Okolna 2, PL-50-422 Wroclaw, Poland

The originality of this thesis has been checked in accordance with the University of Turku quality assurance system using the Turnitin OriginalityCheck service.

ISBN 978-951-29-6670-7 (PRINT)
ISBN 978-951-29-6671-4 (PDF)
ISSN 0082-7002 (Print)
ISSN 2343-3175 (Online)
Painosalama Oy - Turku, Finland 2016

PREFACE

Life is smiling. That is the uppermost feeling I have now thinking how I got at this point where I am about to finish the Doctor of Philosophy degree in chemistry. How cool is that? Of course there have also been some not so glorious moments along the way but who cares – the good ones matter more. I am happy, and a bit surprised to be honest, to see that writing the thesis was not that bad after all. Actually I must admit I even had a lot of fun working with it and the days, and the summer, went really fast.

The work was done mainly at the Laboratory of Materials Chemistry and Chemical Analysis of the University of Turku, during the years 2013-2016, within the Doctoral Programme in Physical and Chemical Sciences, in Turku, Finland. Some measurements were done at the University of the Free State (Bloemfontein, South Africa) and at HASYLAB/DESY (Hamburg, Germany).

The work was funded by University of Turku Graduate School, Academy of Finland (*mobility funding from Finland to South Africa* and projects *Energy Storage Luminophors 2* and *Novel Rare Earth Optical Sensors and Materials* – a bilateral project of Academy of Finland and CNPq, Brazil), and Nordic Energy Research (*AquaFEED* project). All the financiers are gratefully acknowledged. I also want to thank Professor Maarit Karppinen and Dr. Sebastian Vielhauer for the thorough pre-examination, valuable comments and kind words, and Dr hab. Dariusz Hreniak for agreeing to be my opponent. Moreover, there is many other people I want to acknowledge as well.

First of all, I am more than grateful for my supervisors Docent Mika Lastusaari and Dr. Techn. Jorma Hölsä for making everything possible and for all the help, guidance and advices. Thank you for the good discussions and countless hours you have used to assist and teach me. Without your help the publications and this thesis would not exist. I also want to thank all the other co-authors for the help and valuable comments.

I want to thank all the former and current colleagues and friends from our laboratory. Especially I wish to thank Laura Pihlgren and Emilia Palo for teaching me everything and for the warm welcome to the laboratory, and also Ari Lehtonen, Iko Hyppänen, Lucas Rodrigues, José Carvalho, Liana Nakamura, Hellen Santos, Minnea Tuomisto, Isabella Norrbo, Pasi Salonen, Milla Suominen and everyone else, for the excellent working atmosphere and nice discussions. Special thanks go also to Kari Loikas, Kaisa Ketomäki, Mauri Nauma and Kirsi Laaksonen for all the technical and administrative support enabling us to concentrate on research.

One of the best experiences during these years was the possibility to work three months in South Africa at the University of the Free State. For that I am very grateful for Professor Hendrik Swart who kindly invited and allowed me to work at the laboratory and provided a lot of valuable measurement time. I also want to thank Mart-Mari Duvenhage and Elizabeth Coetsee-Hugo for all the measurements and also making my visit so much nicer and fun. I am also very grateful for everyone else for making me feel very welcome.

I am sure we all can agree that life would not be anything without good friends so I want to thank my best friends, Aleksis Mattsson, Kalle Virta, Kristian Lautkoski, Hanna-Mari Salmia, Marica Engström, Minnea Tuomisto, Jasmin Moussa and Olli Moisio, for all the fun we have had during these years, and also for the support and company during the difficult times. I hope we will keep in touch for a long time!

I want to express my deepest gratitude to my mother, father and brothers. Thank you for the outstanding childhood, support and trust. I am happy I have been able to do and study whatever I want without feeling any pressure.

Finally, Hanna, thank you for bringing so much love and joy in my life, as well as for all the help with the thesis.

Turku, November 28, 2016

Tero Laihinen

Tero Laihinen

TABLE OF CONTENTS

ABSTRACT

UNIVERSITY OF TURKU
Faculty of Mathematics and Natural Sciences, Department of Chemistry, Laboratory of Materials Chemistry and Chemical Analysis

LAIHINEN, TERO: Lanthanide doped $NaYF_4$ up-conversion luminescence materials
Doctoral thesis, 118 p.
November 28, 2016

The thesis includes literature and experimental parts. The first part introduces the reader to the topic while the later part contains synthesis and characterization details, results and publications. Up-conversion (UPC) luminescence materials are very interesting and they have plenty of potential applications of which bioanalytical ones are probably the most promising.

A lot of research has been done to study and develop UPC luminescence materials and lanthanide (Ln) doped $NaYF_4$ is maybe the most popular - especially Yb^{3+},Er^{3+} doped $NaYF_4$. The trivalent lanthanides are very good for UPC luminescence due to their ladder-like energy level structures and long excited state lifetimes. Er^{3+}, Tm^{3+} and Ho^{3+} activators are the best ones and often they are used together with an Yb^{3+} sensitizer which enhances the UPC efficiency. Moreover, $NaYF_4$ is considered as the best host.

The aim of this work was to prepare, study and improve UPC luminescence materials based on $NaYF_4$. Yb^{3+} was used as the sensitizer and Pr^{3+}, Nd^{3+}, Sm^{3+}, Eu^{3+}, Tb^{3+}, Dy^{3+}, Ho^{3+}, Er^{3+} and Tm^{3+} were used as activators. The materials were prepared with co-precipitation synthesis and studied with TG-DSC, XPD, TEM, TOF-SIMS, XPS and EXAFS. UPC luminescence was studied under 976 nm excitation.

The synthesis was optimized so that the obtainable luminescence intensity is now even 2 orders of magnitude stronger than before. Several factors contributing to differences between the old and the new improved material were found: The cubic-to-hexagonal phase transition temperature is *ca.* 100 °C lower. The crystal structure is always hexagonal. The particles are covered with sodium. There are less lattice strains. The Na site is partly occupied with Yb^{3+} ions which enhances the Yb^{3+}-Ln^{3+} energy transfer. In the end, UPC luminescence is obtained from all the lanthanides except Sm^{3+} and Dy^{3+}.

TIIVISTELMÄ

TURUN YLIOPISTO
Matemaattis-luonnontieteellinen tiedekunta, Kemian laitos,
Materiaalikemian ja kemiallisen analyysin laboratorio

LAIHINEN, TERO: Lantanideilla seostetut $NaYF_4$-pohjaiset up-konversioluminesenssimateriaalit
Väitöskirja, 118 s.
28. marraskuuta 2016

Väitöskirja sisältää kirjallisen ja kokeellisen osan. Kirjallinen osa johdattelee lukijan aiheeseen ja kokeellinen osa sisältää tiedot valmistus- ja tutkimusmenetelmistä sekä tulokset ja julkaisut. Up-konversioluminesenssimateriaalit ovat erittäin mielenkiintoisia ja niillä on useita potentiaalisia sovelluskohteita joista bioanalyyttiset sovellukset vaikuttaisivat olevan lupaavimpia.

Up-konversioluminesenssimateriaaleja on tutkittu ja kehitetty paljon ja lantanideilla (Ln) seostetut $NaYF_4$-materiaalit ovat ehkä kaikkein suosituimpia - erityisesti Yb^{3+},Er^{3+} seostettu $NaYF_4$. Kolmivalenssiset lantanidit sopivat erittäin hyvin up-konversioluminesenssiin, koska niillä on tikapuumaiset energiatilarakenteet ja virittyneiden tilojen eliniät ovat riittävän pitkiä. Er^{3+}-, Tm^{3+}- ja Ho^{3+}-aktivaattorit ovat parhaimpia ja usein niiden kanssa käytetään Yb^{3+}-herkistintä mikä parantaa up-konversion tehokkuutta. $NaYF_4$:a pidetään parhaimpana pohja-aineena.

Työn tarkoitus oli valmistaa, tutkia ja parantaa $NaYF_4$:iin pohjautuvia up-konversioluminesenssimateriaaleja. Yb^{3+}-herkistintä ja seuraavia aktivaattoreita käytettiin: Pr^{3+}, Nd^{3+}, Sm^{3+}, Eu^{3+}, Tb^{3+}, Dy^{3+}, Ho^{3+}, Er^{3+} ja Tm^{3+}. Materiaalit valmistettiin kerasaostusmenetelmällä ja niitä tutkittiin TG-DSC, XPD, TEM, TOF-SIMS, XPS ja EXAFS menetelmillä. Up-konversioluminesenssia tutkittiin 976 nm virityksellä.

Synteesiä optimoitiin, minkä seurauksena luminesenssin intensiteetti on nyt jopa kaksi kertalukua voimakkaampi kuin ennen. Vanhan ja uuden parannellun materiaalin ominaisuuksissa havaittiin useita eroavuuksia: Kuutiollinen-heksagoninen rakennemuutoslämpötila on nyt n. 100 °C matalampi. Kiderakenne on aina heksagoninen. Partikkelit ovat natriumin peitossa. Hilajännityksiä on vähemmän. Na-paikka on osittain täytetty Yb^{3+}-ioneilla mikä parantaa Yb^{3+}-Ln^{3+}-energiansiirtoa. Nyt up-konversioluminesenssia voidaan havaita kaikista muista lantanideista paitsi Sm^{3+}:sta ja Dy^{3+}:sta.

LIST OF ORIGINAL PUBLICATIONS

The experimental part of the thesis is based on the following publications and supplementary unpublished results. The publications can be found at the end and are referred to in the text by their Roman numerals.

I. Brito, H.F., Hölsä, J., Laamanen, T., Laihinen, T., Lastusaari, M., Rodrigues, L.C.V., Pihlgren, L., and Soukka, T., Rare Earth Distribution in $NaRF_4$: Effect on Up-Conversion Intensity, *Powder Diffr.* **28** (2013) S41-S50.

II. Brito, H.F., Hölsä, J., Laamanen, T., Laihinen, T., Lastusaari, M., Pihlgren, L., Rodrigues, L.C.V., and Soukka, T., EXAFS Study of Cation Reordering in $NaYF_4$:Yb^{3+},Tb^{3+} Up-Conversion Luminescence Materials, *J. Rare Earths* **32** (2014) 226-229.

III. Hölsä, J., Laihinen, T., Laamanen, T., Lastusaari, M., Pihlgren, L., Rodrigues, L.C.V., and Soukka, T., Enhancement of the Up-Conversion Luminescence from $NaYF_4$:Yb^{3+},Tb^{3+}, *Physica B* **439** (2014) 20-23.

IV. Hölsä, J., Laamanen, T., Laihinen, T., Lastusaari, M., Pihlgren, L., and Rodrigues, L.C.V., White Up-Conversion Luminescence of $NaYF_4$:Yb^{3+},Pr^{3+},Er^{3+}, *Opt. Mater.* **36** (2014) 1627-1630.

V. Laihinen, T., Lastusaari, M., Pihlgren, L., Rodrigues, L.C.V., and Hölsä, J., Thermal Behaviour of the $NaYF_4$:Yb^{3+},R^{3+} Materials, *J. Thermal Anal. Calorim.* **121** (2015) 37-43.

VI. Laihinen, T., Palo, E., Pihlgren, L., Rodrigues, L.C.V., Swart, H.C., Lastusaari, M., and Hölsä, J., Comprehensive Up-Conversion Luminescence Tuning Through Selective Lanthanide Doping of $NaYF_4$, a manuscript.

ABBREVIATIONS AND SYMBOLS

2θ	Bragg´s angle
3D	Three dimensional
A	Area
A_{uc}	Absorbance
A/D	Analog-to-digital
APTE	Addition de photons par transfert d'énergie
CCD	Charge-coupled device
CIE	Commission internationale de l'éclairage
CPS	Counts per second
cryo-TEM	Cryo-transmission electron microscopy
d	Mean crystallite size
D	Crystallite size
d^*	Reciprocal d spacing (= $2\sin\theta/\lambda$)
DESY	Deutsches Elektronen-Synchrotron
DSC	Differential scanning calorimetry
E	Energy
E_0	Edge energy
E_s	Intensity of excitation light not absorbed by the sample
E_r	Intensity of excitation light not absorbed by the reference
EDS	Energy-dispersive X-ray spectroscopy
EDTA	Ethylenediaminetetraacetic acid
EDX	Energy-dispersive X-ray spectroscopy
EELS	Electron energy loss spectroscopy
em	Emission
ESA	Excited state absorption
ETU	Energy transfer up-conversion
eUCQY	External up-conversion quantum yield
EXAFS	Extended X-ray absorption fine structure
exc	Excitation
FWHM	Full width at half maximum
GSA	Ground state absorption

h	Planck constant
$h\nu_{max}$	Maximum phonon energy
HAADF	High-angle annular dark-field
HASYLAB	Hamburger Synchrotronstrahlungslabor
HRTEM	High-resolution transmission electron microscopy
I	Irradiance
ICP-MS	Inductively coupled plasma mass spectrometry
IR	Infrared
iUCQY	Internal up-conversion quantum yield
k	Photoelectron wave vector
k_B	Boltzmann constant
KDP	KH_2PO_4
L_s	Emission intensity of the sample
Ln	Lanthanide
NIR	Near infrared
ppm	Parts per million
R	Rare earth
r.m.s.	Root mean square
S.H.G.	Second harmonic generation
SAED	Selected area electron diffraction
SDD	Silicon drift detector
STEM	Scanning transmission electron microscopy
t	Time
TEM	Transmission electron microscopy
TG	Thermogravimetry
TOF-SIMS	Time-of-flight secondary ion mass spectrometry
TPA	Two-photon absorption excitation
UCQY	Up-conversion quantum yield
UV	Ultraviolet
w	Full width at half maximum
x_c	Center
x_{Ln}	Mole fraction of a lanthanide dopant
XPD	X-ray powder diffraction

XPS	X-ray photoelectron spectroscopy
XRD	X-ray diffraction
y_0	Base
β	Full width at half maximum
ΔE	Energy gap
ΔK	Relative reflection broadening
$\Delta\theta$	Half of full width at half maximum
ε	Strain
θ	Angle
λ	Wavelength
ν	Frequency
φ_{abs}	Photon flux of absorbed photons
φ_{in}	Photon flux of incident photons
φ_{uc}	Photon flux of up-converted photons
ω	Multiphonon relaxation rate

1. INTRODUCTION

Lanthanides (Ln), often unknown elements even for some chemists, are very versatile and widely used in everyday applications including fluorescent lamps, displays and security markings in euro notes – not to mention the scientific field. A new research area where lanthanides are also essential is up-conversion luminescence where lower energy radiation, *e.g.* infrared (IR), is converted to higher energy radiation such as visible or even ultraviolet (UV) radiation.[1–3] In other words, two or more low-energy photons are converted to one high-energy photon. Up-conversion luminescence materials have many established and potential applications including lasers,[4–6] displays,[7] security printing,[8] solar cells,[9–13] enhancing photosynthesis,[14] bioimaging[15–20] and biodetection.[21–23]

The unique ladder-like energy level structures of trivalent lanthanides are ideal for up-conversion luminescence and it has been obtained of almost every lanthanide. Er^{3+}, Tm^{3+} and Ho^{3+} are the most efficient ones showing strong UV, blue, green, red and IR luminescence. To minimize cross-relaxation processes lowering the efficiency, the concentration of the emitting ion, *i.e.* activator, must be relatively low (a few percent at the most). Therefore, a host lattice such as $NaYF_4$ must be used to dilute the concentration of the activator. However, a sensitizer (*e.g.* Yb^{3+}) with higher concentration can be used to enhance the efficiency by increasing the absorption. In $NaYF_4$, the lanthanide dopants substitute the Y^{3+} ions with similar size and valence well with even high concentrations.

In theory, an activator with n energy levels could absorb and stack n photons before a radiative emission. However, often only emissions followed by absorption of two or three photons are obtained due to the decreasing efficiency of the up-conversion mechanisms with increasing amount of photons involved in the process. Also for example small

energy gaps between energy levels, short lifetimes and cross-relaxation processes weaken the up-conversion luminescence, as does small crystallite size.

Small nanocrystals with sizes well below 100 nm have attracted a lot of attention due to their high potential especially for bioanalytical applications but the decreasing efficiency with decreasing size is a problem for many applications. Thus, many have studied and developed up-conversion luminescence materials further to enhance the efficiency. For example adding a shell to the particles to hinder the surface quenching have shown good results but there is still work to do. Many different synthesis methods have been developed to produce high-quality lanthanide doped $NaYF_4$ up-conversion luminescence materials. We have used a co-precipitation method[24], because it is simple and fast, to study lanthanide doped $NaYF_4$ up-conversion luminescence materials.

As a result, we were able to modify the synthesis to produce materials showing stronger up-conversion luminescence than before. The details behind this enhancement were studied using transmission electron microscopy (TEM), thermogravimetry (TG), differential scanning calorimetry (DSC), X-ray powder diffraction (XPD), extended X-ray absorption fine structure (EXAFS), time-of-flight secondary ion mass spectrometry (TOF-SIMS) and X-ray photoelectron spectroscopy (XPS). Finally, up-conversion luminescence of praseodymium, neodymium, samarium, europium, terbium, dysprosium, holmium, erbium and thulium was studied in the $NaYF_4$ host in the presence of the ytterbium sensitizer under 976 nm excitation.

The experimental part of the thesis includes details of the materials' preparation and characterization methods (section 4), and the main results (section 5). Moreover, the original publications, referred to in the text with the Roman numerals I-VI, can be found in the end. But first, the following section introduces you to the truly fascinating field of up-conversion luminescence with some additional details.

2. LITERATURE REVIEW

2.1. Basic Requirements for Up-conversion Luminescence

The main requirements for efficient up-conversion luminescence are the following: a ladder-like energy level structure with matching energy differences between the levels and the intermediate energy levels must have long enough lifetimes to enable the stacking of photons.[1-3] Moreover, the energy difference to the energy level below the intermediate energy level, participating to the up-conversion process, should be big enough to avoid efficient multiphonon de-excitation. The multiphonon relaxation rate (ω) decreases exponentially with increasing energy gap (ΔE):[25,26]

$$\omega \propto e^{\frac{-k_B \Delta E}{h\nu_{max}}} \qquad (1)$$

where k_B is the Boltzmann constant and $h\nu_{max}$ is the maximum phonon energy (lattice or impurities). Therefore, the radiative and non-radiative photon and phonon emissions, respectively, are competing processes and high phonon energies can be harmful for the luminescence.

Almost all the trivalent lanthanides fulfill these requirements more or less well (Figure 1) – depending on the excitation energy of course. Due to the use of the Yb^{3+} sensitizer, maybe the most common excitation energy is *ca.* 10200 cm^{-1} (*ca.* 980 nm). Using this amount of energy for example, just by looking at the energy level diagram, Pr^{3+}, Nd^{3+}, Sm^{3+}, Dy^{3+}, Ho^{3+}, Er^{3+} and Tm^{3+} seem to be the best candidates to be an activator while the others do not have any intermediate energy levels even close to the $^2F_{5/2}$ level of Yb^{3+}.

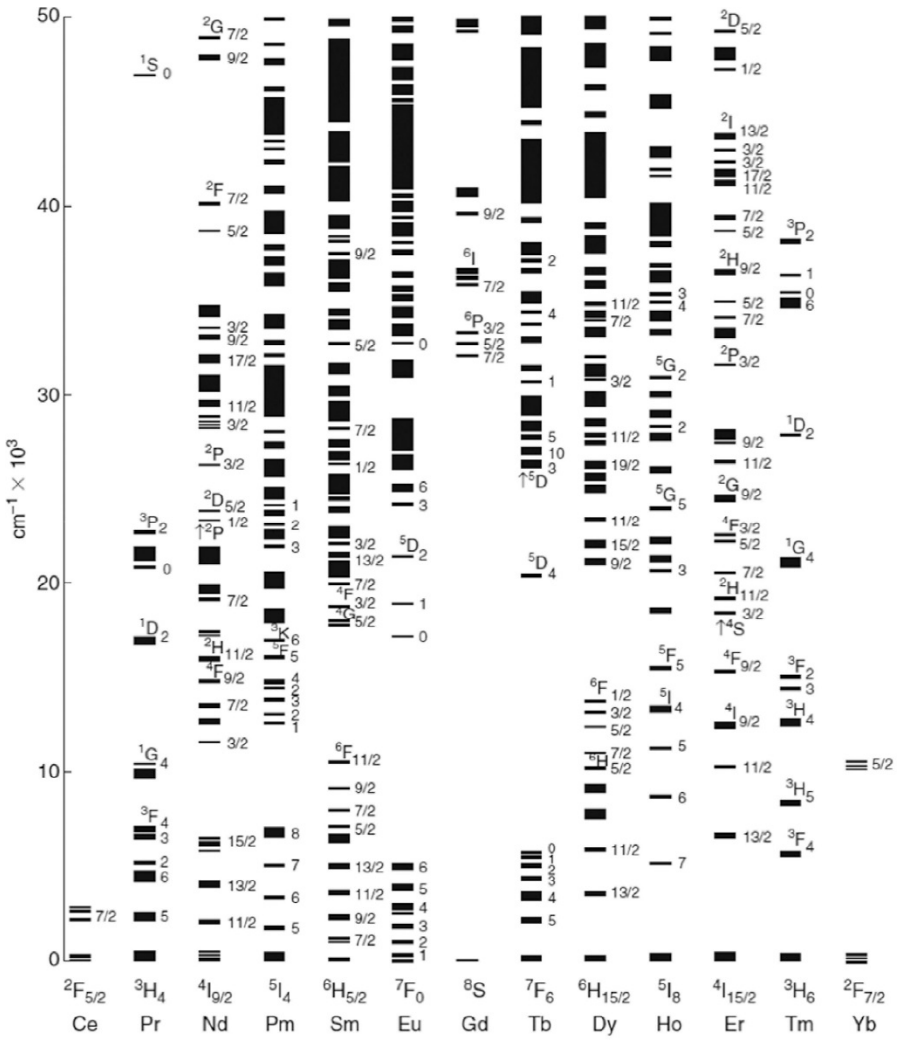

Figure 1. The 4f energy levels of the trivalent lanthanide ions below 50000 cm^{-1}.[27–29]

The high amount of the energy levels (Figure 1) exposes the lanthanides to cross-relaxation processes which can quench the luminescence and change the intensity ratios of the emissions (Figure 2).[1,2] Cross-relaxation means that energy transfers between two similar ions of which at least one is already excited. The result is that one ion de-excites to a lower energy level and the other ion excites to a higher energy level. The probability of the cross-relaxation processes increases with

increasing concentration because then the ions are closer and energy transfer becomes more probable. Therefore, there is an optimum concentration for every lanthanide giving the strongest up-conversion luminescence. Usually it is on the scale of couple percent.

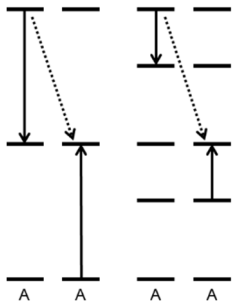

Figure 2. Cross-relaxation mechanisms between two identical activator ions (A).

2.2. Up-conversion Luminescence Mechanisms

There are several different up-conversion mechanisms such as energy transfer up-conversion (ETU) which is referred to also as APTE (addition de photons par transfert d'énergie), two-step absorption (ground state absorption (GSA) followed by excited state absorption (ESA)), cooperative sensitization, cooperative luminescence, second harmonic generation (S.H.G.) and two-photon absorption excitation (TPA; Figure 3).[1]

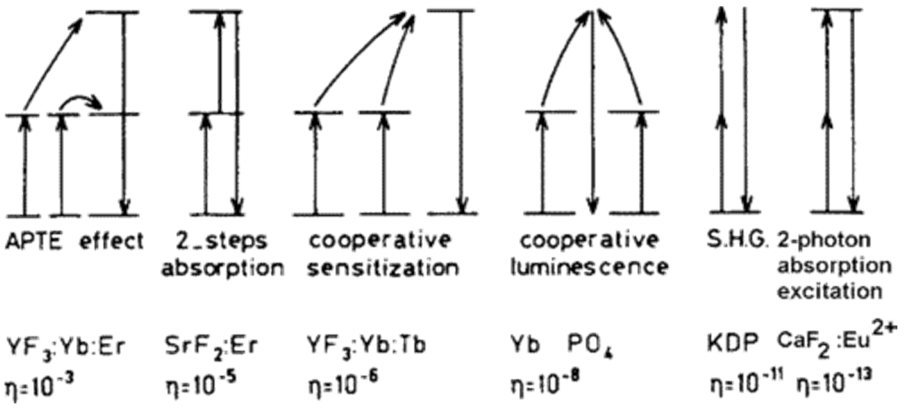

Figure 3. Various two-photon up-conversion processes with their relative efficiency in the specified materials (KDP: KH_2PO_4).[1]

The ETU (APTE) mechanism is clearly the most efficient one for up-conversion. It includes three ions: two sensitizers (*e.g.* Yb^{3+}) and an activator (*e.g.* Er^{3+}). First a sensitizer is excited and subsequently it relaxes back to the ground level and its energy is transferred to an activator which is now excited. Then the other sensitizer transfers a second photon to the same activator while it is still excited. As a consequence, the activator has excited to an energy level with higher energy than the excitation source by absorbing two photons. Finally, the activator can absorb more energy and excite to even higher energy levels or it can relax back to the ground level.

The two-step absorption mechanism, which is often referred to as the ESA mechanism, is the second most efficient one. The difference to ETU is that it does not include sensitizers. Therefore, the mechanism includes only one ion (*e.g.* Er^{3+}) which absorbs two (or more) photons before relaxing back to the ground level.

The cooperative sensitization mechanism has the same principle as ETU but the activator (*e.g.* Tb^{3+}) does not have an intermediate energy level able to absorb a photon from the sensitizer (*e.g.* Yb^{3+}). Therefore, two sensitizers have to transfer the photons at the same time to the activator. Then the activator can excite to an energy level with energy corresponding to two excitation photons. The efficiency of the

cooperative sensitization mechanism is already several orders of magnitude weaker compared to the ETU mechanism due to the lack of the appropriate intermediate energy levels and the cooperative luminescence, S.H.G. and TPA mechanisms are even much more inefficient.

2.3. Ytterbium Sensitizer

Evidently the best efficiency of the Yb^{3+}-Er^{3+} ETU mechanism (several orders of magnitude better than the others) is due to the Yb^{3+} sensitizer. It has only one excited 4f energy level (Figure 1) resulting in an absorption band at around 980 nm due to the $^2F_{7/2} \rightarrow {}^2F_{5/2}$ transition. The absorption cross-section of the Yb^{3+} $^2F_{5/2}$ level is rather good – at least several times better than that of the Er^{3+} $^4I_{11/2}$ level also at *ca.* 980 nm.[30] Moreover, while the activator concentration must be kept low (below *ca.* 5 %) to avoid cross-relaxation processes quenching up-conversion luminescence, the sensitizer concentration can be higher (up to even 100 %)[31] resulting in more efficient absorption and subsequent energy transfer to activator ions.

2.4. Lanthanide Activators

Up-conversion luminescence has been observed from almost every trivalent lanthanide:[32] praseodymium, neodymium, samarium, europium, gadolinium, terbium, dysprosium, holmium, erbium, thulium and even of ytterbium with only one excited 4f energy level. These typical lanthanide activators show up-conversion luminescence emissions at near infrared (NIR), visible and even UV wavelengths (Table 1).

Table 1. Typical lanthanide up-conversion luminescence activators and corresponding up-conversion emissions (modified from)[32].

Activator	Emissions / nm	Corresponding Transitions	References
Pr^{3+}	470, 485, 520, 540, 580, 605, 635, 645, 670, 690 and 720	$^3P_{1,0} \rightarrow {}^3H_4$, $^3P_{1,0} \rightarrow {}^3H_5$, $^3P_{1,0} \rightarrow {}^3H_6$, $^1D_2 \rightarrow {}^3H_4$, $^3P_0 \rightarrow {}^3F_2$, $^3P_1 \rightarrow {}^3F_3$, $^3P_0 \rightarrow {}^3F_3$ and $^3P_0 \rightarrow {}^3F_4$	33–40
Nd^{3+}	430, 482, 525, 535, 580, 600, 664 and 766	$^2P_{1/2} \rightarrow {}^4I_{9/2\text{-}13/2}$, $^4G_{7/2} \rightarrow {}^4I_{9/2}$, $^2P_{1/2} \rightarrow {}^4I_{15/2}$, and $^4G_{7/2} \rightarrow {}^4I_{11/2\text{-}15/2}$	41–47
Sm^{3+}	520, 541, 555, 590, 646, 657, 700 and 799–873	$^4G_{7/2} \rightarrow {}^6H_{5/2}$, $^4F_{3/2} \rightarrow {}^6H_{5/2}$, $^4G_{5/2} \rightarrow {}^6H_{5/2}$, $^4G_{5/2} \rightarrow {}^6H_{7/2}$, $^4G_{7/2} \rightarrow {}^6H_{9/2}$, $^4G_{5/2} \rightarrow {}^6H_{9/2}$, $^4G_{5/2} \rightarrow {}^6H_{11/2}$ and $^6F_{11/2} \rightarrow {}^6H_{5/2}$	48–52
Eu^{3+}	416, 429, 490, 510, 535, 554, 590 and 613	$^5D_3 \rightarrow {}^7F_1$, $^5D_3 \rightarrow {}^7F_2$, $^5D_2 \rightarrow {}^7F_2$, $^5D_2 \rightarrow {}^7F_3$, $^5D_1 \rightarrow {}^7F_1$, $^5D_1 \rightarrow {}^7F_2$, $^5D_0 \rightarrow {}^7F_1$ and $^5D_0 \rightarrow {}^7F_2$	52–58
Gd^{3+}	278, 305 and 312	$^6I_{7/2} \rightarrow {}^8S_{7/2}$, $^6P_{5/2} \rightarrow {}^8S_{7/2}$ and $^6P_{7/2} \rightarrow {}^8S_{7/2}$	52,59
Tb^{3+}	381, 415, 438, 489, 541, 584 and 619	$^5D_3 \rightarrow {}^7F_6$, $^5D_3 \rightarrow {}^7F_5$, $^5D_3 \rightarrow {}^7F_4$, $^5D_4 \rightarrow {}^7F_6$, $^5D_4 \rightarrow {}^7F_5$, $^5D_4 \rightarrow {}^7F_4$ and $^5D_4 \rightarrow {}^7F_3$	52,56,60–67
Dy^{3+}	378, 408, 487, 543, 569, 570, 610, 655 and 663	$^4G_{11/2,9/2} \rightarrow {}^6H_{13/2}$, $^4G_{9/2} \rightarrow {}^6H_{11/2}$, $^4I_{15/2} \rightarrow {}^6H_{13/2}$, $^4G_{11/2} \rightarrow {}^6H_{111/2}$, $^4F_{9/2} \rightarrow {}^6H_{13/2}$, $^4G_{11/2} \rightarrow {}^6H_{9/2}$, $^4G_{11/2} \rightarrow {}^6H_{7/2}$ and $^4F_{9/2} \rightarrow {}^6H_{11/2}$	52,68–75
Ho^{3+}	360, 391, 412, 490, 542, 655 and 754	$^5G_2,{}^3K_7 \rightarrow {}^5I_8$, $^5G_{4,6} \rightarrow {}^5I_8$, $^5F_{2,3} \rightarrow {}^5I_8$, $^5S_2 \rightarrow {}^5I_8$, $^5F_5 \rightarrow {}^5I_8$ and $^5S_2 \rightarrow {}^5I_7$	58,62,76–79
Er^{3+}	415, 525, 542, 655 and 848	$^2H_{9/2} \rightarrow {}^4I_{15/2}$, $^2H_{11/2} \rightarrow {}^4I_{15/2}$, $^4S_{3/2} \rightarrow {}^4I_{15/2}$, $^4F_{9/2} \rightarrow {}^4I_{15/2}$ and $^4S_{3/2} \rightarrow {}^4I_{13/2}$	57,66,77,80–83
Tm^{3+}	290, 345, 362, 450, 475, 644, 694 and 800	$^1I_6 \rightarrow {}^3H_6$, $^1I_6 \rightarrow {}^3F_4$, $^1D_2 \rightarrow {}^3H_6$, $^1D_2 \rightarrow {}^3F_4$, $^1G_4 \rightarrow {}^3H_6$, $^1G_4 \rightarrow {}^3F_4$, $^3F_3 \rightarrow {}^3H_6$ and $^3H_4 \rightarrow {}^3H_6$	59,63,77,84–88
Yb^{3+}	450–500	$2 \times {}^2F_{5/2} \rightarrow {}^2F_{7/2}$ (cooperative emission)	89,90

If one think about the energy level schemes (Figure 1), up-conversion processes (Figure 3) and the key requirements for up-conversion luminescence,[1–3,32] it seems quite clear why up-conversion luminescence is so strong especially for Er^{3+}. Its $^4I_{15/2} \rightarrow {}^4I_{11/2}$ transition is in very good resonance with the energy of Yb^{3+} $^2F_{5/2}$ level enabling the most efficient ETU mechanism. The energy difference between the intermediate energy level and the lower level is big and there is no quenching cross-relaxation process. Moreover, the absorption of the second photon ($^4I_{11/2} \rightarrow {}^2F_{7/2}$ transition) is also efficient due to very good energy resonance. Therefore, Er^{3+} fulfils all the main requirements very well. Also Tm^{3+} and Ho^{3+} show strong up-conversion luminescence through the ETU mechanism.

The rest of the lanthanides produce weaker up-conversion luminescence compared to Er^{3+}, Tm^{3+} and Ho^{3+} even in the presence of the Yb^{3+} sensitizer.[1–3,32] Trivalent praseodymium,[33,34] samarium[51] and dysprosium[74,75] can excite with the ETU mechanism but the nonradiative relaxation mechanisms weaken the efficiency. Pr^{3+} has several efficient cross-relaxation processes (Equations 2-4) that can de-excite it nonradiatively back to the $^3H_4$ ground level. Sm^{3+} and Dy^{3+} have small energy differences between the energy levels below the *ca.* 10000 cm^{-1} excitation energy (Figure 1) resulting in efficient nonradiative multiphonon de-excitation.

$$(^1G_4,{}^3H_4) \rightarrow (^3H_5,{}^3F_4),\ (^3H_6,{}^3F_2),\ (^3F_2,{}^3H_6) \text{ or } (^3F_4,{}^3H_5) \qquad (2)$$

$$(^1D_2,{}^3H_4) \rightarrow (^1G_4,{}^3F_4) \text{ or } (^3F_4,{}^1G_4) \qquad (3)$$

$$(^3P_0,{}^3H_4) \rightarrow (^1G_4,{}^1G_4) \text{ or } (^1D_2,{}^3H_6) \qquad (4)$$

Moreover, neodymium[46,47] excites via the ESA mechanisms (λ_{exc}: 532 or 797 nm) which is less efficient than the ETU mechanism, europium and terbium excite through the even less efficient cooperative sensitization mechanism[56] due to the lack of appropriate intermediate energy levels (Figure 1) and the up-conversion luminescence of

ytterbium[89] occurs due to the most inefficient mechanism, cooperative luminescence. Gadolinium has the first excited level at *ca.* 32000 cm^{-1},[26,91] well above the energy of NIR radiation, and thus the Yb^{3+} sensitizer cannot transfer energy straight to Gd^{3+}. Therefore, Tm^{3+} has been used as an additional sensitizer and Yb^{3+}-Tm^{3+}-Gd^{3+} energy transfer have been obtained.[59]

2.5. Up-conversion Quantum Yield

Up-conversion quantum yield (UCQY) is considerably smaller than luminescence quantum yield which has been reported to be as high as 85 %.[92,93] Whereas even in theory the maximum internal UCQY (iUCQY) is only 50, 33 and 100/n % for two, three and n photon processes, respectively.[94,95] In practice the iUCQY is with current nanomaterials only about a few percent at the most and often *ca.* 0.1-1 % even under high power excitation (Table 2). Moreover, the UCQY decreases rapidly with decreasing crystallite size and for example the iUCQY of a $NaYF_4$:Yb^{3+},Er^{3+} material drops about 95 % (from 0.10 to 0.005 %) when the crystallite size decreases from 30 to 10 nm (67 % decrease).[94] Adding a $NaYF_4$ shell to the $NaYF_4$:Yb^{3+},Er^3 core improved the iUCQY by 200 % but was still only 0.30 % with 30 nm crystallites.

Table 2. iUCQY and normalized iUCQY values of up-conversion luminescence materials with different sizes, wavelengths and irradiance (modified from)[96].

Materials	Size (with shell) / nm	λ_{exc} / nm	Irradiance / Wcm^{-2}	iUCQY / %	Normalized iUCQY / cm^2W^{-1}	Reference
β-$NaYF_4:Er^{3+}/\beta$-$NaLuF_4$	19.2 (38.8)	1523	0.43 ± 0.03	0.71 ± 0.08	0.017 ± 0.002	97
β-$NaYF_4:Er^{3+}/\beta$-$NaLuF_4$ in PMMA	19.2 (38.8)	1523	0.43 ± 0.03	2.01 ± 0.19	0.047 ± 0.005	97
β-$NaYF_4:Er^{3+}/\beta$-$NaYF_4$	22 (25/38)	1532	18	0.7	$3.9 * 10^{-4}$	98
$LiYF_4:Er^{3+}$	85	1490	150	1.2 ± 0.1	$8 * 10^{-5}$	99
β-$NaYF_4:Yb^{3+},Er^{3+}$	100	980	150	0.3 ± 0.1	$2 * 10^{-5}$	94
β-$NaYF_4:Yb^{3+},Er^{3+}$	30	980	150	0.10 ± 0.05	$<6 * 10^{-5}$	94
β-$NaYF_4:Yb^{3+},Er^{3+}$	8–10	980	150	0.005 ± 0.005	$<4 * 10^{-7}$	94
β-$NaYF_4:Yb^{3+},Er^{3+}/\beta$-$NaYF_4$	30	980	150	0.30 ± 0.10	$2 * 10^{-5}$	94
β-$NaYF_4:Yb^{3+},Er^{3+}$	300	980	50	0.05 ± 0.02	$1 * 10^{-5}$	100
$LiYF_4:Yb^{3+},Er^{3+}$	16	976	60 mW laser	0.04	-	101
$LiYF_4:Yb^{3+},Er^{3+}$	27	976	60 mW laser	0.14	-	101
$LiYF_4:Yb^{3+},Er^{3+}$	200	976	60 mW laser	0.3	-	101
β-$NaYF_4:Yb^{3+},Er^{3+}$	200	972	380 mW laser	0.05 to 0.255	-	102
β-$NaYbF_4$: Tm^{3+}/CaF_2	20 (27)	980	0.3	0.6 ± 0.1	0.02	103
β-$NaYF_4:Yb^{3+},Tm^{3+}/\beta$-$NaYF_4$	30 (42)	980	78	3.5	$<5 * 10^{-4}$	104

The iUCQY of a microcrystalline $NaYF_4:Er^{3+}$ has been reported to be even 12 ± 1.0 % under low irradiance of 0.40 ± 0.02 Wcm^{-2} at 1523 nm meaning that the normalized iUCQY is 0.3 cm^2W^{-1}.[97,105] Therefore, more studies are needed to improve the efficiency of the nanomaterials. It is therefore important to know how small crystallites you really need to avoid unnecessary decrease in the up-conversion luminescence intensity. Even though some researchers think the quantum efficiency of up-conversion luminescence materials is too low for practical use, up-conversion luminescence materials are already good enough for at least some bioanalytical applications such as the commercial Upcon™ concept developed by Kaivogen Oy, Finland and Labrox Oy, Finland.[106]

UCQY can be measured using two different methods: external UCQY (eUCQY) and iUCQY.[13,96,97] The eUCQY and iUCQY describe the efficiency of the material and up-conversion process, respectively. The UCQY values depend on the excitation power density because up-conversion luminescence is a nonlinear process, *i.e.* at least two excitation photons are needed for one emission photon.[95,96] Therefore, also normalized UCQY values, which take into account the power dependency, are used. The UCQY methods are defined as:[1,13,94–97,107,108]

$$eUCQY = \frac{\phi_{uc}}{\phi_{in}} \tag{5}$$

$$iUCQY = \frac{\phi_{uc}}{\phi_{abs}} = \frac{1}{A_{uc}} eUCQY = \frac{L_s}{E_r - E_s} \tag{6}$$

$$normalized\ UCQY = \frac{UCQY}{I} \tag{7}$$

where ϕ_{uc}, ϕ_{in} and ϕ_{abs} are the photon fluxes of the up-converted, incident and absorbed photons, respectively. A_{uc} is the absorbance of the sample, L_s is the emission intensity of the sample, E_s and E_r are the

intensities of the excitation light not absorbed by the sample and the reference sample, respectively, and I is the irradiance of the excitation.

An integrating sphere is usually used to ensure that all emitted, transmitted and reflected radiation is collected (Figure 4).[94–96,107,109] Both absolute and relative quantum yield measurements are used but due to the lack of reliable reference samples the absolute measurements are more reliable if the system is properly calibrated.[94,96,109] This includes the calibration of the monochromators, detectors as well as the integrating sphere.[94] All in all, measuring the UCQY reliably can be challenging and thus often UCQY values are not presented. However, such a method, using a commercially available spectrophotometer, has been presented for example by Boyer and van Veggel.[94]

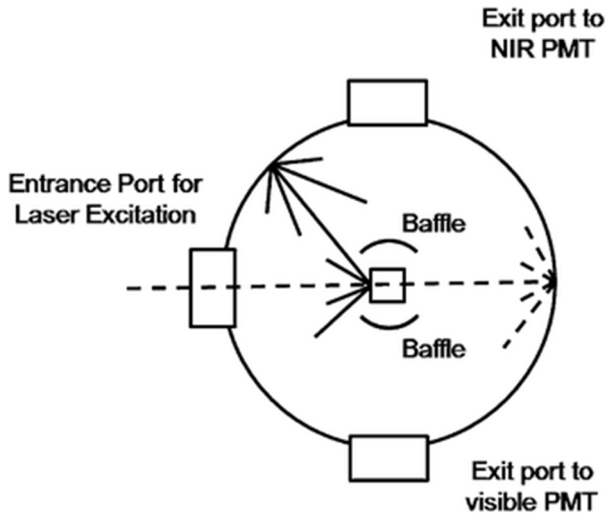

Figure 4. Diagram of an integrating sphere setup for luminescence measurements. Dashed and solid line represent excitation light and sample emission, respectively.[94]

2.6. Sodium Yttrium Tetrafluoride

Lanthanide doped $NaYF_4$ materials have three different crystal structures:[110,111] low- and high-temperature cubic fluorite (CaF_2) type structure ($Fm\bar{3}m$, #225, Z: 2)[112], as well as hexagonal structure ($P6_3/m$, #176, Z: 1.5)[113] at the intermediate temperatures (Figure 5). The structure

changes as a function of temperature and is cubic at low and high temperatures and hexagonal at the intermediate temperatures. The exact phase transition temperatures depend on the synthesis, dopants and dopant concentrations but the hexagonal form is usually obtained after heat treatment around 300-600 °C. However, hexagonal particles have also been prepared at room temperature.[114]

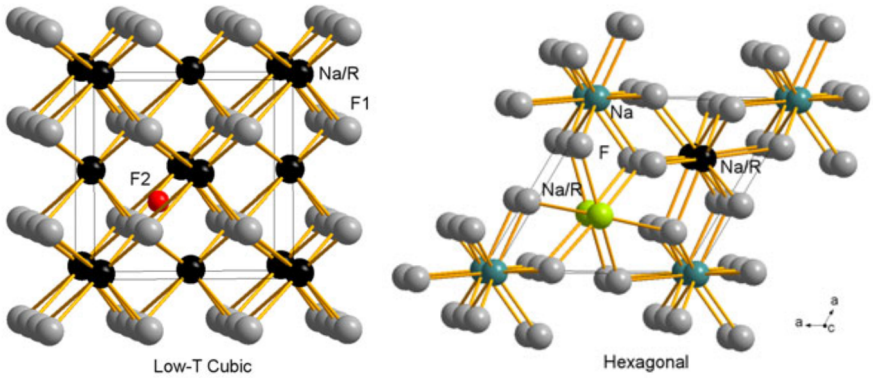

Figure 5. Unit cells of low-temperature cubic and hexagonal $Na(Y_{0.80}Yb_{0.17}Er_{0.03})F_4$ (R: rare earth).[111]

The cubic forms have one cation site (coordination number is VIII) occupied with Na, Y and Ln ions which are partially in order (low-temperature structure) or randomly distributed (high-temperature structure).[111] Due to the Y/Ln enriched stoichiometry, there is an additional interstitial fluoride site with *ca.* 4 % occupancy.[111] The symmetry of the cation site is C_{3v} (low-temperature cubic) or O_h (high-temperature cubic structure).

The hexagonal structure has one fluoride site and two cation sites: the first one is occupied with Na (coordination number is VI) and the second one is shared with Na, Y and Ln (coordination number is IX).[111] The symmetries of the cation sites are C_{3h} (Na site) and C_3 (Na/Y/Ln site). 60 % of the Na ions occupy the Na site and therefore 40 % the Na/Y/Ln site. Unlike the cubic structures, the hexagonal one is close to stoichiometric.

The cubic forms are not as good as the hexagonal one for up-conversion luminescence and thus the hexagonal form is usually preferred.[3,84,115–117] One difference between the cubic and hexagonal forms is the more compact structure of the hexagonal form resulting in shorter distances between lanthanides enabling more efficient energy transfer.[111] The hexagonal form is considered to be among the best hosts for efficient up-conversion luminescence – if not the best one.[3,84,115–118]

The hexagonal form has outstanding properties such as low phonon energy of the crystal lattice (*ca.* 500 cm^{-1} max[118–120]), two different lattice sites for the dopant ions,[116,118] and the quite similar effective ion sizes of Na^+, Y^{3+} and trivalent lanthanide dopants (the size differences are less than 18 % compared to Na^+;[121] Table 3). The weighted average of the phonon energy of $NaYF_4$ is only *ca.* 360 cm^{-1},[119] the phonon energies of $NaYF_4$ and $NaLnF_4$ (Ln: La, Ce, Pr, Sm, Eu or Gd) materials are under 500 cm^{-1},[120] and therefore also $NaYF_4$ material doped with Yb^{3+} and Er^{3+} have similar (under 500 cm^{-1}) phonon energies.[118] The low phonon energy hinders the nonradiative multiphonon de-excitation processes[25,26] (section 2.1) which results in long lifetimes of the excited states.[3] The two possible lattice sites for the dopants increases the probability of the energy transfer from a sensitizer to an activator.[116] The similar cation sizes prevents the formation of lattice defects and stress.[3]

Table 3. Effective ion sizes of Na^+, Y^{3+} and trivalent lanthanides with coordination numbers VIII (cation site in the cubic) and IX (Na/Y/Ln cation site in the hexagonal structure; modified from)[121].

Ion	Effective Ionic Radius / Å		Size Difference Compared to Na^+ / %	
	VIII	IX	VIII	IX
Na^+	1.18	1.24	-	-
Y^{3+}	1.019	1.075	-13.6	-13.3
Ce^{3+}	1.143	1.196	-3.1	-3.5
Pr^{3+}	1.126	1.179	-4.6	-4.9
Nd^{3+}	1.109	1.163	-6.0	-6.2
Pm^{3+}	1.093	1.144	-7.4	-7.7
Sm^{3+}	1.079	1.132	-8.6	-8.7
Eu^{3+}	1.066	1.120	-9.7	-9.7
Gd^{3+}	1.053	1.107	-10.8	-10.7
Tb^{3+}	1.040	1.095	-11.9	-11.7
Dy^{3+}	1.027	1.083	-13.0	-12.7
Ho^{3+}	1.015	1.072	-14.0	-13.5
Er^{3+}	1.004	1.062	-14.9	-14.4
Tm^{3+}	0.994	1.052	-15.8	-15.2
Yb^{3+}	0.985	1.042	-16.5	-16.0
Lu^{3+}	0.977	1.032	-17.2	-16.8

2.6.1. *Tuning Characteristic Properties*

Nowadays high-quality lanthanide doped $NaYF_4$ materials can be prepared in different structural forms, crystallite sizes and shapes (Figure 6) by tuning *e.g.* the Na/(Y+Ln) ratio, solvent, temperature and reaction time.[24,114,122–134] For example the particle size of cubic $NaYF_4$ has been doubled from 9 to 18 nm by doubling the NaF/Y^{3+} ratio from 5 to 10,[126] and the amount of the cubic phase of $NaYF_4$:Yb,Er has been decreased and finally vanished by adding Gd^{3+} as a co-dopant.[127] Moreover, adding chelating agents such as ethylenediaminetetraacetic acid (EDTA) can have a big effect on the particle size by forming metal-EDTA complexes

resulting in smaller particle size and narrower size distribution (section 2.6.2).[24]

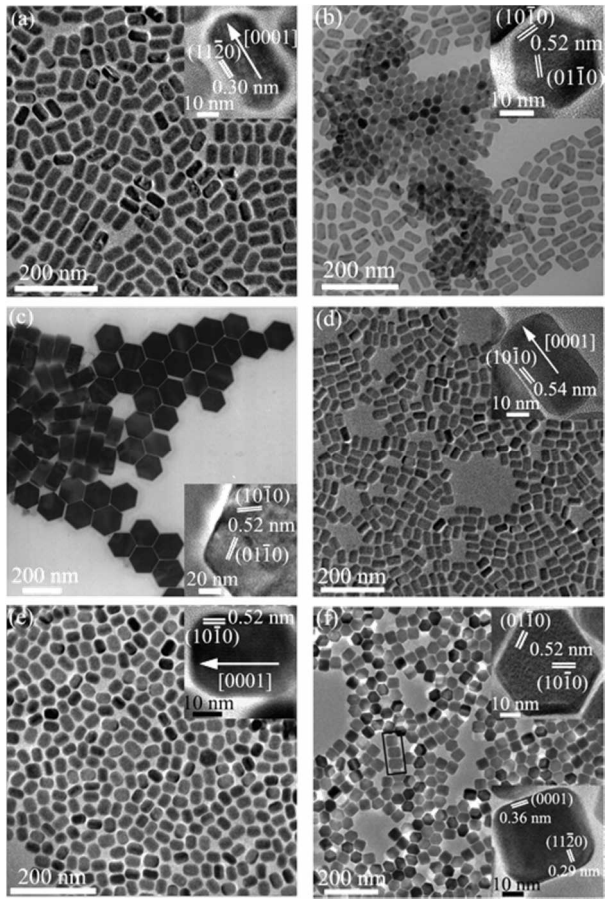

Figure 6. TEM and HRTEM (inset) images of β-$NaYF_4$ nanorods redispersed in toluene/hexane (1:1) (a) and in toluene/hexane/ethanol (1:1:0.48) (b), of β-$NaYF_4$ nanoplates (c), of β-$NaNdF_4$ nanorods (d), and of β-$NaEuF_4$ nanorods (e). TEM and HRTEM (inset, upper: lying flat on the face; lower: standing on the side face from the highlighted square) images of β-$NaHoF_4$ hexagonal plates (f).[122]

Also co-doping for example with Mn^{2+} has a big effect on the structural form and crystallite size of lanthanide doped $NaYF_4$ materials.[19,135] Adding Mn^{2+} favors the formation of the cubic form (adding 5 % or more Mn^{2+} shows only the cubic form) and the crystallite

size can be tuned by changing Mn^{2+} concentration. Interestingly, the Mn^{2+} co-doping has also a huge effect on the red-to-green ratio (increases from 1 to 160) of the Er^{3+} up-conversion luminescence: doping 30 mol-% Mn^{2+} quenches the green emissions almost entirely while the red emission becomes stronger (Figure 7 left). This has been attributed to be due to nonradiative energy transfers from Er^{3+} to Mn^{2+} and then back to Er^{3+} feeding the $^4F_{9/2}$ level emitting red luminescence (Figure 7 right). Moreover, the Mn^{2+} doping increases the up-conversion luminescence intensity which has been presented to be due to changes in the activator environment and the energy transfers between Er^{3+} and Mn^{2+}.

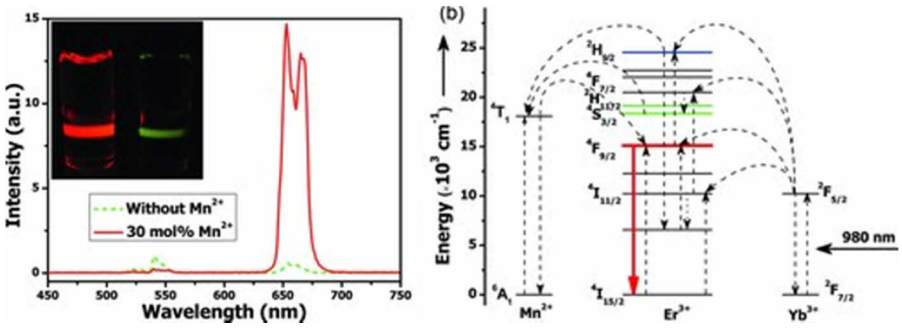

Figure 7. Room temperature upconversion emission spectra of $NaYF_4$:Yb/Er (18/2 mol-%) nanocrystals with 0 and 30 mol-% Mn^{2+} dopant ions dispersed in cyclohexane (1 mg/dm^3; left). Inset shows the corresponding luminescent photographs. Schematic energy level diagram showing the possible upconversion mechanism of Mn^{2+}-doped $NaYF_4$:Yb/Er nanocrystals (right).[19]

2.6.2. *Co-precipitation Synthesis*

$NaYF_4$:Yb^{3+},Ln^{3+} nanomaterials can be prepared with several different techniques and co-precipitation[24] is one of the simplest ones. Thus we chose to use this synthesis in the present experimental work. The synthesis is carried out by mixing aqueous solutions of NaF, YCl_3 and $LnCl_3$ (Ln: Yb and a lanthanide activator) and EDTA at room temperature to form metal-EDTA complexes. The precipitate is separated by centrifuging, washed with water and ethanol, dried, annealed for five hours at desired temperature (*ca.* 400-600 °C) under

H_2/N_2 gas sphere and cooled down to room temperature. With the co-precipitation synthesis, the particle size can be controlled effectively from 37 to 166 nm by chancing the molar ratio of EDTA and Ln^{3+} (Figure 8). However, impurity cubic form is observed when EDTA is used. This weakens the up-conversion luminescence and thus EDTA is sometimes not used in the synthesis.

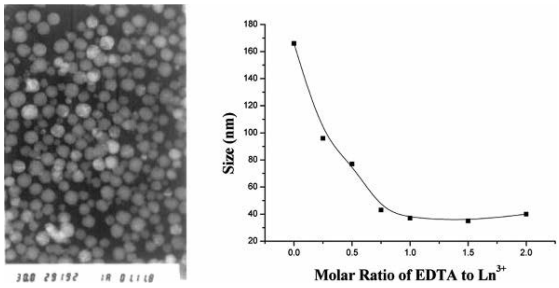

Figure 8. TEM image of as-prepared $NaYF_4$:Yb,Er nanoparticles prepared with co-precipitation synthesis using a molar ratio of 1:1 EDTA/lanthanides (left) and relationship between TEM particle size and EDTA/Ln^{3+} ratio (right).[24]

2.6.3. *Core-shell Concept*

The nanoscale size of the up-conversion luminescence particles is preferred in many applications but unfortunately nanoparticles have weaker efficiency compared to corresponding bulk materials (section 2.5) due to the bigger surface to volume ratio resulting in surface quenching.[136] Moreover, the molecules on the surface such as OH^- of water can quench the luminescence due to multiphonon de-excitation processes.[137,138] OH^- for example has several times higher phonon energies (*ca.* 3500 cm^{-1}) compared to the lattice phonons of the hexagonal $NaYF_4$ (*ca.* 500 cm^{-1} max[118–120]) which increases the probability of the multiphonon de-excitation.

To avoid the quenching, different core-shell structures have been studied to protect the dopants contributing to the up-conversion luminescence process and both passive[82,94,136,138–144] (*e.g.* silica or undoped host) and active[52,145–149] (*e.g.* host with dopants) shells have been studied. However, the core-shell interface may also, and probably will, contain

quenching sites which complicates the core-shell method. Anyway in many cases (*e.g.* bio applications) some kind of surface modification of the up-conversion luminescence nanoparticles is usually required to make them for example water dispersible and compatible with biological substrates and a silica shell is a common starting point.

High quality core-shell materials with a narrow size distribution can be prepared using for example a layer-by-layer method to grow the shell, using Ostwald ripening dynamics, on nanocrystals prepared by using *e.g.* an oleic acid synthesis (Figure 9).[140,143] The shell thickness increases by *ca.* 1 nm with every layer which allows the fine tuning of the shell thickness. Moreover, each layer increases the up-conversion luminescence intensity showing the protective effect of the shell. All in all, the core-shell concept has proven to be an efficient method to enhance the luminescence properties of the lanthanide doped $NaYF_4$ up-conversion luminescence nanomaterials.

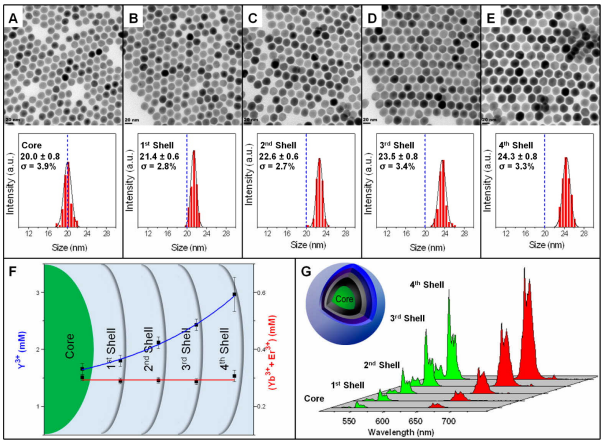

Figure 9. (A–E) TEM images and size distribution of $NaYF_4$:Yb^{3+}/Er^{3+} (15/2 %) core nanocrystals (t = 0), $NaYF_4$:Yb^{3+}/Er^{3+} (15/2 %) core/$NaYF_4$ shell nanocrystals after successive layer-by-layer epitaxial growth at t = 5, 10, 15, and 20 min, respectively; (F) ICP-MS (inductively coupled plasma mass spectrometry) elemental analysis of the core and core–shell nanocrystals with same number concentration of nanocrystals; (G) upconversion emission spectra of the hexane dispersions of core and core–shell nanocrystals with same number concentration of nanocrystals under 980 nm excitation.[143]

2.6.4. *Basic Characterization Methods*

Lanthanide doped $NaYF_4$ up-conversion luminescence materials are commonly characterized by using XPD, TEM and luminescence spectroscopy including decay and power dependence measurements.[35,57–59,67,81,82,84,85,87] XPD is used to determine the crystal from (cubic and/or hexagonal), the presence of crystalline impurities (*e.g.* NaF and NaCl) and crystallite size by using the Scherrer formula (when smaller than *ca.* 100 nm):[150,151]

$$d = \frac{0.9\lambda}{\beta \cos\theta} \qquad (8)$$

where d (m) is the mean crystallite size, λ (m) is the wavelength of the incident X-rays and θ (°) is half of the Bragg´s angle (2θ). Moreover, β is the full width at half maximum (FWHM) of the reflection after eliminating the broadening due to the instrument:

$$\beta^2 = \beta_s^2 - \beta_r^2 \qquad (9)$$

where s and r refers to the sample and microcrystalline reference, respectively.

TEM can be used to study the particle size and morphology. The decay and power dependence measurements are used to study excitation and energy transfer mechanisms. Up-conversion luminescence intensity increases linearly, in a log-log diagram, as a function of excitation power and the slope of the fitting curve reveals the amount of photons involved in the process: the slope is *ca.* 2, 3 and n for two, three and n photon processes, respectively.

The formation of the core-shell structure can be shown by using XPS, cryo-transmission electron microscopy (cryo-TEM), scanning transmission electron microscopy (STEM), energy-dispersive X-ray spectroscopy (EDS or EDX), electron energy loss spectroscopy (EELS) and high-angle annular dark-field (HAADF) methods (Figure 10).[140,152,153]

Moreover, several indirect characterization methods such as selected area electron diffraction (SAED), TEM, high-resolution TEM (HRTEM) and X-ray diffraction (XRD) have been used to evaluate if a core-shell structure is formed.[82,144,147,149]

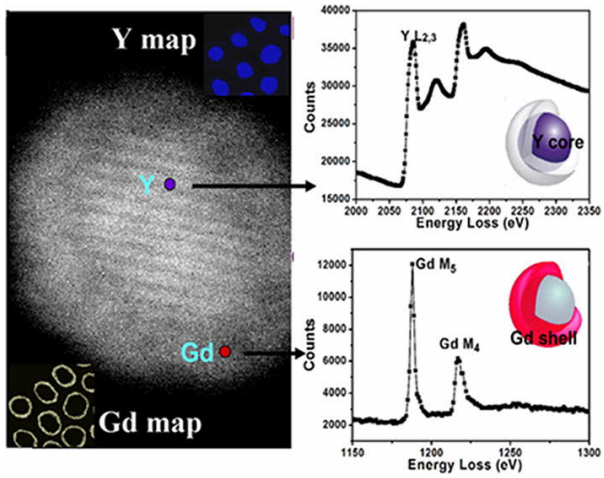

Figure 10. HAADF image of a single $NaYF_4$:Yb,Er@$NaGdF_4$ nanocrystal (left). The insets show the corresponding chemical maps and reveal the presence of yttrium at the nanocrystals center (blue) and gadolinium at the periphery of nanocrystals (yellow). EELS spectra of yttrium $L_{2,3}$ (right up) and gadolinium $M_{4,5}$ (right down) edges taken from the probe location on the inferred $NaYF_4$:Yb,Er core and $NaGdF_4$ shell (left) using the nanocrystal with 6 monolayers $NaGdF_4$ shell.[140]

3. AIMS OF THE EXPERIMENTAL WORK

The aim of the experimental work was to study and improve the properties of lanthanide (Pr, Nd, Sm, Eu, Tb, Dy, Ho, Er, Tm and Yb were used) doped $NaYF_4$ up-conversion luminescence materials. The properties were studied comprehensively using novel methods such as TG-DSC, XPD, TEM, TOF-SIMS, XPS, EXAFS, and luminescence spectroscopy. The main research topics were the following:

1. Improving the co-precipitation synthesis to produce pure hexagonal $NaYF_4$:Yb^{3+},Ln^{3+} materials (Publications I-III).

2. Studying the structural details causing the up-conversion luminescence enhancement (I and II).

3. Improving the up-conversion luminescence efficiency (I-III).

4. The role of the Er^{3+} impurity on the up-conversion luminescence efficiency and color (III and IV).

5. Phase transition temperatures and behaviour under heating (V).

6. Up-conversion luminescence of lanthanides (III, IV and VI).

7. Utilizing the improved synthesis and up-conversion luminescence efficiency (VI).

4. MATERIALS AND METHODS

4.1. Materials Preparation

Yttrium and lanthanide oxides (Table 4) were dissolved in hydrochloric acid (pro analysi, 37 %, Sigma Aldrich) and diluted with quartz distilled water to prepare aqueous YCl_3 and $LnCl_3$ solutions with 0.5 $moldm^{-3}$ Y^{3+}/Ln^{3+} concentration (Equation 10). The pH was adjusted to *ca.* 2. Sodium fluoride (pro analysi, Sigma-Aldrich) and absolute ethanol (99.5 %, Altia) were used as received.

Table 4. The yttrium and lanthanide oxides used to synthesize lanthanide doped $NaYF_4$ materials.

Compound	Formula	Purity* / %	Manufacturer
Yttrium oxide	Y_2O_3	99.99	Sigma-Aldrich
Praseodymium oxide	Pr_6O_{11}	99	Typpi
Neodymium oxide	Nd_2O_3	99.9	Rhône-Poulenc
Samarium oxide	Sm_2O_3	99.9	Rhône-Poulenc
Europium oxide	Eu_2O_3	99.99	Double Pilots Group Holdings
Terbium oxide	Tb_4O_7	99.9	Rhodia
Dysprosium oxide	Dy_2O_3	99.9	Rhodia
Holmium oxide	Ho_2O_3	99.9	Rhodia
Erbium oxide	Er_2O_3	99.99	Aldrich
Thulium oxide	Tm_2O_3	99.9	Rhône-Poulenc
Ytterbium oxide	Yb_2O_3	99.99	Metal Rare Earth

*With respect to other lanthanides.

$$Ln_2O_3(s) + 6HCl(aq) \rightarrow 2LnCl_3(aq) + 3H_2O(l) \qquad (10)$$

$NaYF_4$, $NaYbF_4$, $NaYF_4:Yb^{3+}$ and $NaYF_4:Yb^{3+},Ln^{3+}$ (Ln: Pr, Nd, Sm, Eu, Tb, Dy, Ho, Er or Tm) up-conversion luminescence materials were prepared with selected dopant concentrations (x_{Yb}: 0.10-0.20, x_{Pr}: 0.001-0.01, x_{Nd}: 0.002-0.04, x_{Sm}: 0.002-0.02, x_{Eu}: 0.002-0.04, x_{Tb}: 0.005-0.08, x_{Dy}: 0.002-0.02, x_{Ho}: 0.02, x_{Er}: 0.03 and x_{Tm}: 0.005) using the co-precipitation synthesis[24]. Solid NaF (2.1 g; 0.050 mol) was dissolved to quartz distilled water (60 cm^3). This solution was further mixed with aqueous solution (20 cm^3; 0.010 mol) containing YCl_3, $YbCl_3$ and $LnCl_3$ to obtain the stoichiometry desired (Equation 11). An excess amount of sodium was used to force the formation of the $NaYF_4$ phase instead of the YF_3 and to ensure the formation of the hexagonal crystal form during the post-annealing.

$$YCl_3(aq) + 4NaF(aq) \rightarrow NaYF_4(s) + 3NaCl(aq) \qquad (11)$$

After stirring for one hour at room temperature, the precipitate formed was centrifuged (3766 g) for eight minutes, washed three times with water (3*20 cm^3) and once with ethanol (20 cm^3) or only once with ethanol. Each washing was followed by centrifuging. The precipitate was then dried in a vacuum desiccator at room temperature and a selected amount (*ca.* 0.15 of 0.8 g) of the dry product powder was annealed (Thermo Electron Corporation Lindberg/blue M furnace) inside a quartz glass reactor for five hours at 500 °C under a static N_2 + 10 % H_2 gas sphere. After annealing, the materials were cooled down freely to the room temperature under the same gas sphere. More N_2 + 10 % H_2 gas was added to the quartz reactor during the cooling to prevent replacement air to enter.

4.2. Characterization Methods

4.2.1. *Transmission Electron Microscopy*

The particle size and shape of the $NaYF_4$ materials were analyzed with TEM using a JEM-1400 Plus transmission electron microscope. The acceleration voltage was 80 kV and resolution 0.38 nm. The microscope

was equipped with an OSIS Quemesa 11 Mpix bottom mounted digital camera.

4.2.2. *Thermogravimetry and Differential Scanning Calorimetry*

The thermal behaviour of the as-prepared materials was studied with a TA Instruments SDT Q600 simultaneous TG-DSC apparatus between 25 and 720 °C in flowing N_2 (100 cm^3min^{-1}). The materials were studied with the DSC to determine the cubic-to-hexagonal and hexagonal-to-cubic phase transition temperatures. This information is crucial when selecting the annealing temperature for obtaining the hexagonal crystal form.

A heating rate of 5 °Cmin^{-1} and sample mass of *ca.* 10 mg were used. The sample pan was made of aluminium oxide and a similar but empty pan was used as a reference material. The specific enthalpies of the phase transitions were calculated by integrating the corresponding DSC signals. Selected materials were studied to higher temperatures (up to 1300 °C) and some were also examined during the cooling phase to study the reversibility of the processes occurring during the heating.

4.2.3. *X-ray Powder Diffraction*

The structure and phase purity of the materials were analyzed with XPD measurements by comparing the patterns to the reference patterns of the cubic[112] $NaYF_4$ and hexagonal[113] $Na(Y_{0.57}Yb_{0.39}Er_{0.04})F_4$. The patterns were collected at room temperature with a Huber G670 image plate Guinier camera (2θ range 4–100°, data interval 0.005°) with monochromatic copper $K_{\alpha 1}$ radiation (λ: 1.54056 Å). The effect of the preferred orientation was minimized by oscillating the sample horizontally. The asymmetry of the reflections at low angles is due to the apparatus used. However, this effect can be corrected even for Rietveld structure refinements.

For the Rietveld analyses[154] the dataset was summed from twelve half an hour measurements. The Rietveld analyses were carried out with the FullProf.2k program.[155] The microstrains and crystallite sizes were

calculated from the reflection widths of the whole diffraction patterns by using Williamson-Hall plots,[156,157] which are based on the following equations:

$$\Delta K = \frac{1}{D} + 2\varepsilon d^* \qquad (12)$$

and

$$\Delta K = 2\cos\theta \frac{\Delta\theta}{\lambda} \qquad (13)$$

with ΔK equal to the relative reflection broadening, D is the crystallite size, ε is the strain, d^* is the reciprocal d spacing (= $2\sin\theta/\lambda$) and Δθ is equal to the half of the FWHM (in radians). The crystallite size and the r.m.s. (root mean square) strain were obtained from the intercept and the slope of the ΔK vs. d^* plot, respectively. Silicon powder (NIST standard 640b) was used as the reference for the reflection widths.

4.2.4. *Extended X-ray Absorption Fine Structure*

The environments of Y, Yb and Tb in selected $NaYF_4$:Yb^{3+},Tb^{3+} materials were studied using EXAFS. The measurements were carried out at room temperature at beamlines A1 and C at the DORIS storage ring of HASYLAB (Hamburger Synchrotronstrahlungslabor) at DESY (Deutsches Elektronen-Synchrotron) in Hamburg, Germany.

Data was collected from the Y K, Tb L_{III} and Yb L_{III} edges using a Si(111) double crystal monochromator. The measurements were carried out in a fluorescence mode using a M3 7 pixel silicon drift detector (SDD). The energy range was from -100 to 600 eV with respect to the absorption edge. Steps of 0.3 eV and 0.4 nm^{-1} were used for the data collection at the near edge and extended regions, respectively. The total time per measurement was *ca.* 1 h from which one minute took place before the edge.

The data handling and the extraction of the interatomic distances from the EXAFS data was carried out with the EXAFSPAK program package.[158] For the Fourier transforms, photoelectron wave vector (k; Equation 14 where E_0 is the edge energy) ranges starting from 30 nm^{-1} were used to avoid the increased multiple scattering contributions at lower energies. The end value was set as high as allowed by the data, usually to 120 nm^{-1}.

$$k = \sqrt{0.2625(E - E_0)} \qquad (14)$$

4.2.5. *Time-of-flight Secondary Ion Mass Spectrometry*

The elemental distributions, impurities and depth profiles were studied with TOF-SIMS using a TOF.SIMS 5 spectrometer (IONTOF) with a pulsed 30 keV Bi^+ beam. The measurement area was 100 * 100 μm^2 and sputtering was done with oxygen to obtain three dimensional (3D) images. The TOF-SIMS measurements were kindly provided by Dr. Duvenhage and Prof. Swart (University of the Free State, Bloemfontein, South Africa).

4.2.6. *X-ray Photoelectron Spectroscopy*

The elemental compositions and dopant concentrations were studied with XPS using a PHI 5000 VersaProbe spectrometer with monochromatic Al Kα radiation (E: 1486.6 eV). Survey spectra were measured from 0 to 1400 eV (1 eV/step) and high resolution spectra (0.1 eV/step) were measured in selected narrower energy ranges. The measurements were made from the surface and after 30 s sputtering (*ca.* 18 nm/min). A low energy Ar^+ ion gun and low energy neutralizer electron gun was used to minimize charging on the surface. The XPS measurements were kindly provided by Dr. Coetsee-Hugo and Prof. Swart (University of the Free State, Bloemfontein, South Africa).

The spectra were corrected with the C_{1s} signal at 284.6 eV and the relative atomic concentrations were estimated by calculating the peak

areas from the survey spectra. The Origin 2015 program[159] was used to fit the high resolution XPS spectra using the Gaussian function:

$$y = y_0 + \frac{Ae^{\frac{-4ln(2)(x-x_c)^2}{w}}}{w\sqrt{\frac{\pi}{4ln(2)}}} \qquad (15)$$

where y_0, x_c, A and w are the base, center, area and FWHM, respectively.

4.2.7. *Up-conversion Luminescence and Decay Time*

Up-conversion luminescence spectra were measured from dry powders inside a capillary tube at room temperature with a CCD (charge-coupled device) spectrometer (Ocean Optics PC2000). The NIR excitation (λ_{exc}: 976 nm; ν: 10246 cm^{-1}) source was a continuous wave Hamamatsu L9418-04 laser diode. The optical part of the setup consisted of tubular excitation and emission chambers (Thorlabs) in a right-angle configuration, and an optical fiber to direct emission to the detector. (Figure 11). The spectra were collected with an Ocean Optics OOIIrrad software.

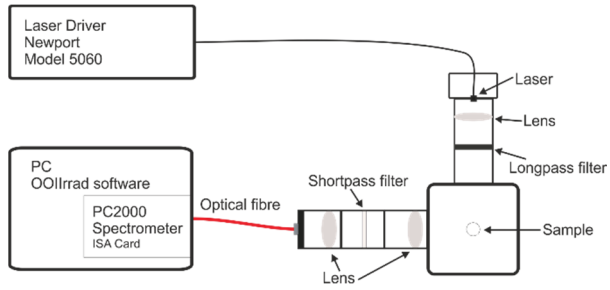

Figure 11. A schematic figure of the up-conversion luminescence measuring setup.

In the excitation light path, a RG850 long-pass filter (Edmund Optics) with a cutoff at 850 nm was used to ensure a pure NIR excitation (Figure 12). In the emission light path, an extended hot mirror filter (Edmund Optics) with a good transmission at the visible wavelengths

was used to exclude the scattered excitation radiation. However, the transmission is poor around 390-420 nm.

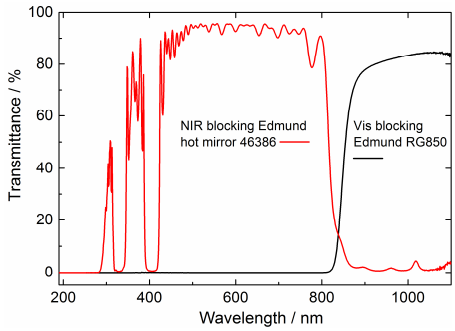

Figure 12. Transmittance spectra of the filters used in the up-conversion luminescence measurements.

Up-conversion luminescence decay curves were measured from dry powders inside a capillary tube at room temperature with a head-on R1464 photomultiplier (Hamamatsu). The excitation source and the optical setup of the excitation side was the same as in the spectral measurements (Figure 11). The optical setup of the emission side was otherwise the same but it included a bandpass filter (Thorlabs FL543.5-10: 543.5 ± 5 nm or Newport 10LF10-488: 488 ± 5 nm) and the optical fiber was replaced by the photomultiplier.

The photomultiplier signal was amplified with a DHPCA-100 high-speed current amplifier (Femto Messtechnik GmbH). The amplified signal was recorded with a NI USB-6251 A/D (analog-to-digital) converter, which was connected to a computer via USB and controlled with a computer program written in LabVIEW 8.5 (National Instruments). The pulse profile consisted of a 1 ms waiting time followed by a 20 ms excitation pulse and a 80 ms delay period after switching of the laser. Therefore, one cycle was 101 ms long. The pulse profile was cycled 10000 times during a single measurement.

5. RESULTS AND DISCUSSION

5.1. Effects of Different Preparation Methods

Since the hexagonal form shows stronger up-conversion luminescence than the cubic forms and the presence of an excess Na is essential during the cubic-to-hexagonal phase transition,[111] the effect of increasing the Na amount was studied. The co-precipitation synthesis includes an excess amount of the NaF precursor but the water washings dissolve most of the excess NaF away. Thus the water washings were omitted to simply increase the amount of the NaF and thus Na present during the post-annealing. The properties and differences of thus prepared lanthanide doped $NaYF_4$ materials with and without the water washings were studied extensively.

5.1.1. *Thermal Behaviour*

The DSC curves show that the phase transitions occur at the same temperature ranges when the same preparation method is used (III, V). The cubic-to-hexagonal transition occurs at 400-450 or 325-375 °C with or without water washings, respectively, and the hexagonal-to-cubic transition occurs at 650-700 °C with both washing methods (III). Thus the cubic-to-hexagonal phase transition temperature is *ca.* 100 °C lower without the water washings due to the presence of the excess NaF which works as a source for the sodium needed for the transition. Whereas with the water washings the sodium deficiency hinders the transition and therefore requires higher temperature. It is also notable that the hexagonal-to-cubic phase transition temperature is almost unaffected by the dopant and its concentration although the cubic-to-hexagonal transition temperature decreases with decreasing dopant size and concentration. After the post-annealing, the materials can be cooled to the room temperature because the phase transitions are irreversible.[160]

The TG measurements show only minor (under 5 %) mass losses below 800 °C (IV, V). The mass change is the fastest at low temperatures (below 300 °C) and can be attributed to occur mainly due to the removal of water, ethanol and possible water of crystallation. Above 300 °C the mass loss is due to the slow evaporation of the NaF. The mass loss rate is small at intermediate temperatures between the phase transition temperatures and thus the annealing is safe regarding the stability of the materials. At higher temperatures the mass decreases strongly and the total mass loss is *ca.* 40 % when heated up to 1200 °C. This is due to the evaporation of the NaF resulting in the decomposition of the $NaYF_4$. However, such high temperatures are not necessary to obtain the hexagonal crystal form.

5.1.2. *Crystal Form and Phase Purity*

The XPD patterns show that with water washings some of the post-annealed materials contain also the cubic form in addition to the hexagonal one (III, V). The presence and amount of the cubic form depends on the dopant and its concentration but no clear correlation was observed (V): For example with the Nd^{3+} and Eu^{3+} doped materials increasing the Ln^{3+} concentration reduced the amount of the cubic form and with the Sm^{3+} and Tb^{3+} doped materials it was the opposite. However, it was found out that if the water washings were omitted, the crystal form of the post-annealed materials was pure hexagonal with no trace of the cubic form (III, VI).

The only drawback of omitting the water washings is the presence of NaF and NaCl impurities (I, III, VI). However, those impurities could probably be washed away after the annealing without harming the material but that must be studied in the future. Anyway, as a result of this finding new materials can be prepared with pure hexagonal structure which is better than the cubic form for efficient up-conversion luminescence. Therefore, a wider selection of lanthanide dopants and concentrations are now obtainable for the $NaYF_4$ host using the same synthesis.

5.1.3. *Particle Size and Shape*

TEM images show clearly that the particle surfaces of the as-prepared $NaYF_4$ materials is smoother with than without the water washings (Figure 13). It seems that the particles are covered with some smaller particles without the water washings and there are also bigger bar and star-like particles. Otherwise the particle shape is quite similar with both washing methods. Based on the XPD studies showing the presence of the excess NaF (I, III, VI), it is probable that the as-prepared $NaYF_4$ particles prepared without the water washings are covered with the NaF. The particle size is *ca.* 200-300 nm independent of the washing method. However, the particle size distribution is not very narrow so there is some smaller and bigger particles as well.

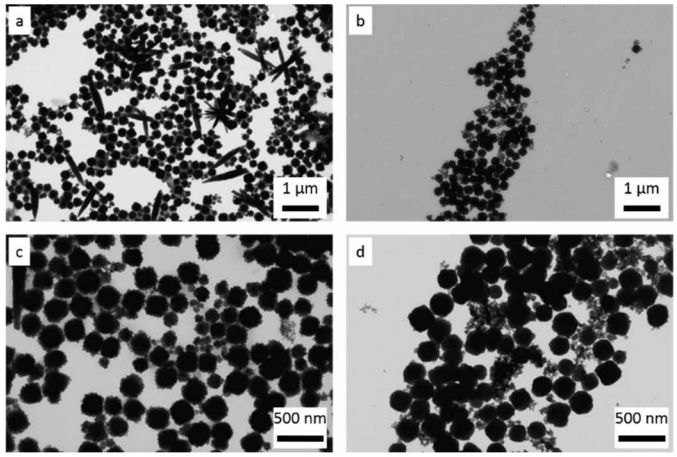

Figure 13. TEM images of the as-prepared $NaYF_4$ materials prepared without (a, c) and with (b, d) the water washings.

After annealing the $NaYF_4$ materials at 500 °C for five hours, the TEM images show aggregated particles with both washings methods (Figure 14). Without the water washings, the particle size is over 500 nm, even 1 µm, which is considerably bigger than the *ca.* 200-300 nm with the water washings. There are also some considerably smaller particles with the water washings which could be for example due to impurity YF_3 phase.

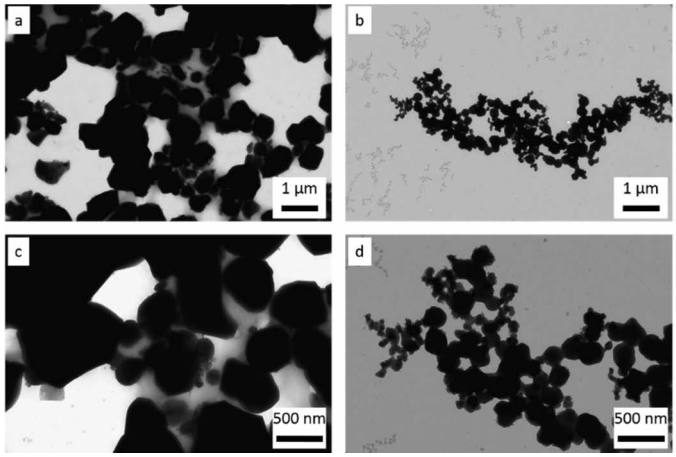

Figure 14. TEM images of the annealed (5 h @ 500 °C) $NaYF_4$ materials prepared without (a, c) and with (b, d) the water washings.

5.1.4. *Elemental Distribution*

3D TOF-SIMS images show that the as-prepared $NaYF_4$ material obtained without the water washings, which have a layer on top of the particles (Figure 13 a and c), clearly have more sodium on the surface compared to the bulk (Figure 15 left). With the corresponding $NaYF_4$ material prepared with the water washings, sodium is more evenly distributed (Figure 15 right). Thus, these results support the hypothesis of the NaF covering the as-prepared $NaYF_4$ materials without the water washings.

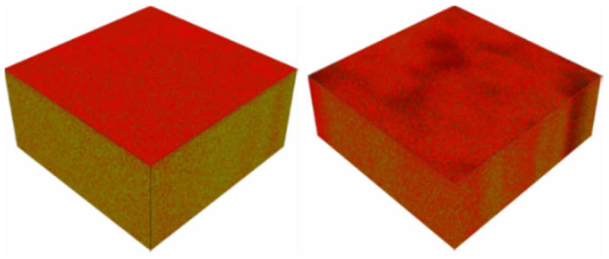

Figure 15. 3D TOF-SIMS overlay images of the as-prepared $NaYF_4$ materials prepared without (left) and with (right) the water washings showing sodium and yttrium with red and green color, respectively (surface area: 100 * 100 μm^2, depth: unknown).

However, the corresponding Yb^{3+}-Tb^{3+} co-doped $NaYF_4$ materials do not show exactly the same kind of behaviour: sodium is more evenly distributed all over the materials (Figure 16). But there is still more sodium on the surface compared to the bulk and the smaller amount of yttrium in the bulk might be just due to the lower concentration of yttrium due to the Yb^{3+}-Tb^{3+} co-doping (total 23 mol-%). In any case, there might be, and probably is, some variation between syntheses.

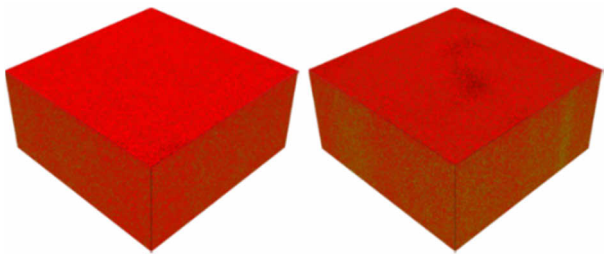

Figure 16. 3D TOF-SIMS overlay images of the as-prepared $NaYF_4$:Yb^{3+},Tb^{3+} materials prepared without (left) and with (right) the water washings showing sodium and yttrium with red and green color, respectively (surface area: 100 * 100 μm², depth: unknown).

The annealed (5 h @ 500 °C) $NaYF_4$ and $NaYF_4$:Yb^{3+},Tb^{3+} materials show much more variation in the sodium concentration compared to the as-prepared materials (Figure 17). Again the surfaces are richer of the sodium than the bulk. However, sodium is distributed quite unevenly especially with the Yb^{3+}-Tb^{3+} co-doped materials and there are spots with very high amounts of sodium going deep below the surface. This could mean that there is some sodium-richer compound among the particles: *e.g.* NaF and/or NaCl which are observed in the XPD measurements (I, III, VI).

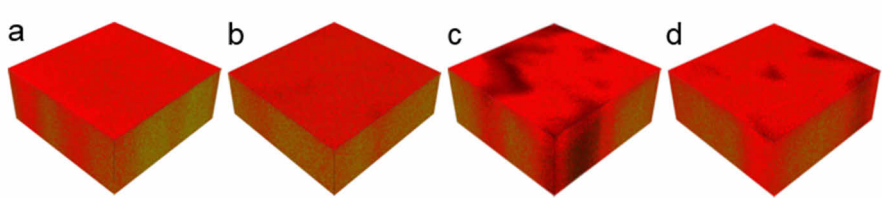

Figure 17. 3D TOF-SIMS overlay images of the annealed $NaYF_4$ (a and b) and $NaYF_4$:Yb^{3+},Tb^{3+} (c and d) materials prepared without (a and c) and with (b and d) the water washings showing sodium and yttrium with red and green color, respectively (surface area: 100 * 100 μm^2, depth: unknown).

More detailed TOF-SIMS image of the surface of annealed $NaYF_4$:Yb^{3+},Tb^{3+} material prepared without the water washings show that the ytterbium and terbium dopants are quite evenly distributed on the same areas with yttrium (Figure 18 left). Moreover, there is always sodium and fluoride wherever there is yttrium (Figure 18 right). Therefore, it is concluded that the dopants have replaced some of the yttrium ions, and $NaYF_4$ and $NaYF_4$:Yb^{3+},Tb^{3+} have been formed as excepted and wanted. Some impurities such as carbon, magnesium, potassium, calcium, titanium, manganese, iron and other lanthanides such as erbium and thulium were observed, as well.

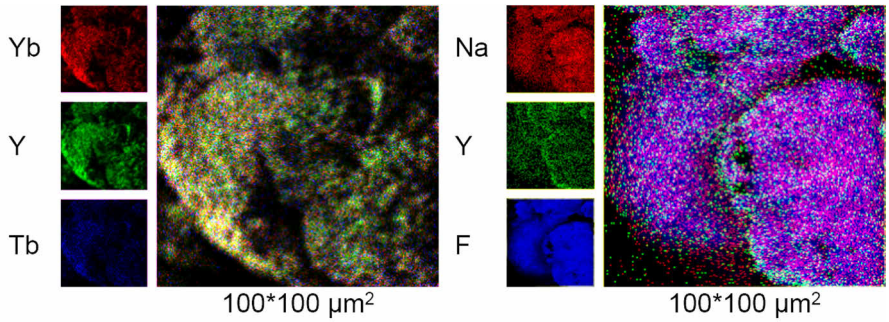

Figure 18. TOF-SIMS images of the annealed $NaYF_4$:Yb^{3+},Tb^{3+} material prepared without the water washings showing ytterbium, yttrium and terbium (as positive ions; left), and sodium, yttrium and fluoride (as negative ions; right) distributions.

5.1.5. *Elemental Composition*

The XPS survey scan spectra of the $NaYF_4$:Yb^{3+},Tb^{3+} materials show the presence of Na, Y, F, Yb and Tb with both washing methods before and after the sputtering (Figure 19). The binding energy peaks of the Na 1s, Y 3d, F 1s, Yb 4d and Tb 3d electrons are observed at *ca.* 1072, 159, 685, 186 and 1240 eV, respectively.[161] However, the Yb and Tb signals are quite weak due to their low concentrations. Also carbon and oxygen impurities are observed at *ca.* 280 and 530 eV, respectively.

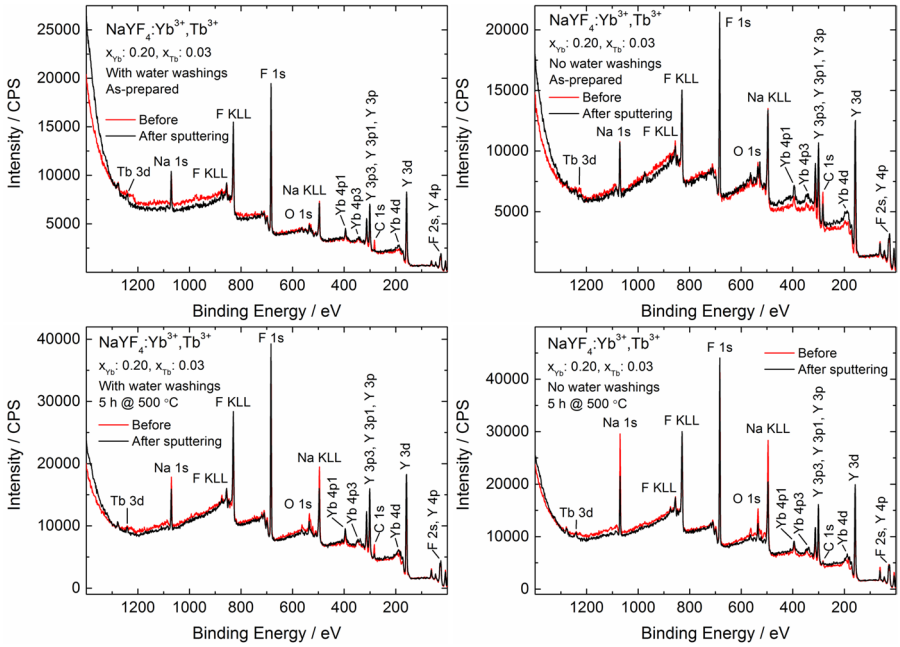

Figure 19. XPS survey scan spectra of the as-prepared (top) and annealed (bottom) $NaYF_4$:Yb^{3+},Tb^{3+} materials prepared with (left) and without (right) the water washings before (red) and after (black) the sputtering.

With the $NaYF_4$:Yb^{3+},Tb^{3+} materials washed with water the atomic concentrations seem to be very similar independent of the conditions: without and with the annealing, before and after the sputtering (Table 5). The only notable difference is the *ca.* 10 percentage point increase and decrease in the fluoride and carbon concentrations, respectively, during

the sputtering. The difference is mainly due to surface impurities such as ethanol used the last in the washings and carbon dioxide absorbed from air.

Table 5. Percentage atomic concentrations of the as-prepared and annealed $NaYF_4:Yb^{3+},Tb^{3+}$ materials prepared with and without the water washings before and after (the bolded values) the sputtering.

Element	Atomic % before and after the sputtering							
	As-prepared				Annealed			
	with water		without water		with water		without water	
Na	13	**16**	4	**9**	15	**13**	28	**19**
Y	14	**14**	16	**20**	14	**16**	12	**15**
F	55	**65**	44	**58**	56	**66**	54	**63**
Yb	2	**2**	2	**<1**	<1	**1**	<1	**1**
Tb	<1	**<1**	<1	**<1**	<1	**<1**	<1	**<1**
C	13	**1**	32	**4**	12	**3**	5	**2**
O	3	**2**	1	**8**	2	**<1**	1	**<1**

With the as-prepared $NaYF_4:Yb^{3+},Tb^{3+}$ material washed without water the atomic concentrations vary more than with the water washed materials (Table 5). The carbon concentration is even almost 30 percentage points (700 %) higher before the sputtering suggesting there is lot of carbon including impurities such as ethanol on the surface. The huge decrease in the carbon concentration during the sputtering results in clear increases in the sodium, yttrium, fluoride and surprisingly also oxide concentrations.

With the annealed $NaYF_4:Yb^{3+},Tb^{3+}$ materials there is a clear difference between the sodium concentrations on the surfaces with both washing methods (Table 5). Without the water washings there is *ca.* 50 % more (9 percentage points) sodium on the surface (before the sputtering) compared to the core (after the sputtering). Whereas with the water

washings there is only *ca.* 15 % more (2 percentage points) sodium on the surface compared to the core.

Therefore, the XPS studies confirm that the particle surfaces of the annealed material prepared without the water washings are richer in sodium than the material prepared with the water washings, as expected. However, surprisingly the as-prepared material without the water washings has very low sodium concentration compared to all other materials even though the corresponding annealed material has the highest sodium concentration. This might be due to the high concentration of impurities (carbon and oxygen) with the as-prepared material without the water washings. Also it should be kept in mind that these are only relative, not absolute, concentrations. Thus comparing different materials might be complicated.

5.1.6. *Chemical Environment*

The high resolution XPS spectra before the sputtering show clearly the typical doublet of yttrium around 160 eV due to the 3d electrons with all the $NaYF_4:Yb^{3+},Tb^{3+}$ materials (Figure 20 left). The peak with higher binding energy belongs to $3d_{3/2}$, and the one with lower energy and higher intensity to $3d_{5/2}$. After the sputtering an additional signal is obtained right next to the yttrium doublet (Figure 20 right) which is due to yttrium with different chemical environment in the material.[162]

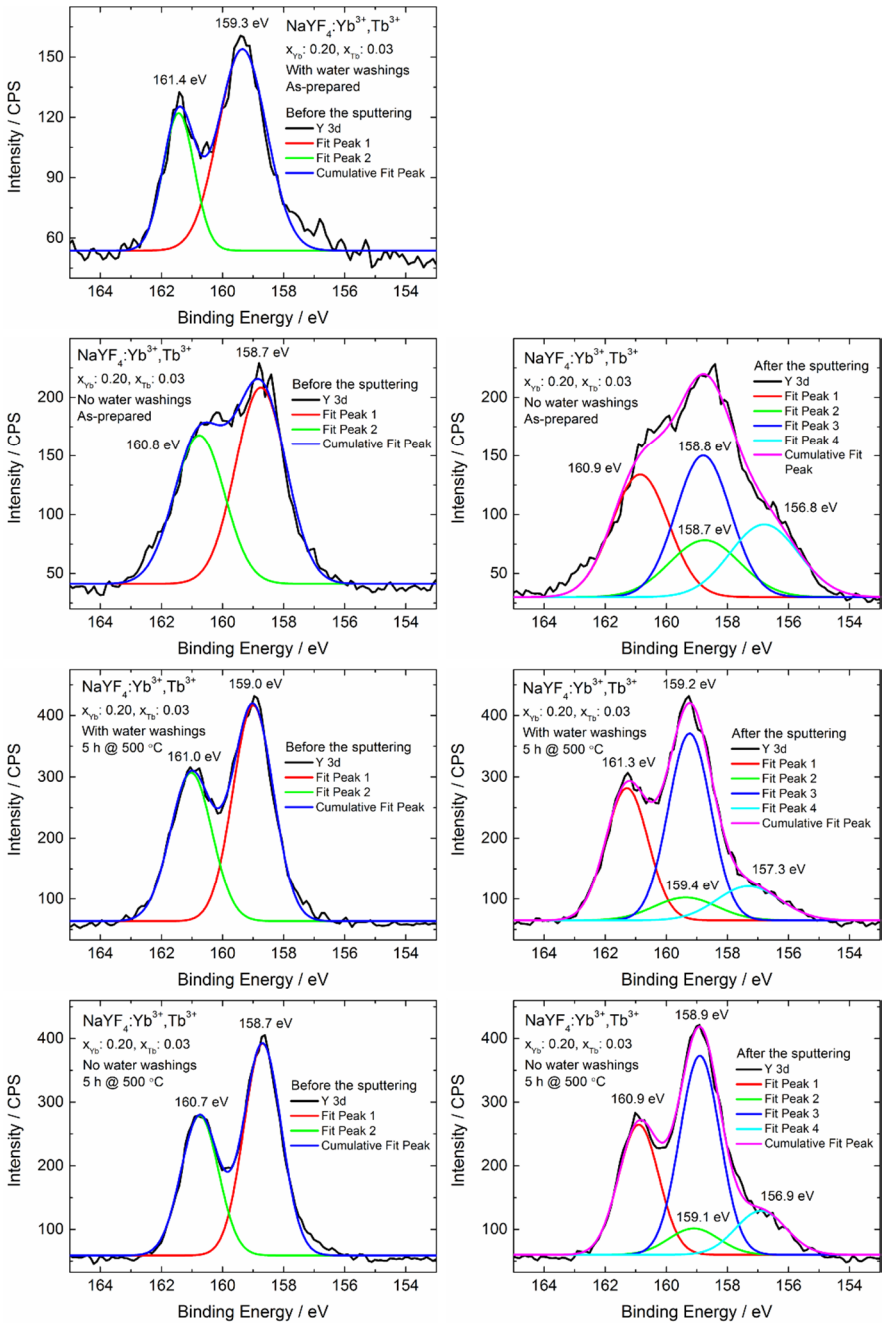

Figure 20. Y (3d) XPS spectra with fitting curves of the as-prepared and annealed $NaYF_4:Yb^{3+},Tb^{3+}$ materials obtained with and without the water washings before (left) and after (right) the sputtering.

The presence of the two yttrium doublets is clearly seen of the fitting curves where two (one doublet) and four peaks (two doublets) are needed before and after the sputtering, respectively. To be more precise, the two doubles are due to yttrium ions on the surface and in the bulk.[162] It is also possible that the two signals are observed because yttrium occupies partly also the Na site in the $NaYF_4$ lattice. No clear difference was obtained between materials with different washing methods. However, the binding energies are slightly higher with the water washings.

The reason why the two doublets are present only (at least more clearly since there might be a barely visible weak peak around 157 eV) after the sputtering could be the lower concentration of impurities on the surface compared to the state before the sputtering. XPS detects mainly ions close to the surface and therefore thicker layer of impurities results in a thinner layer of actual material being measured. This could explain also why the yttrium 3d signal of the as-prepared materials have lower intensity, and signal-to-noise ratio, than with the annealed materials (Figure 20) since the as-prepared materials have higher concentration of impurities (Table 5) and a layer on top of the particles (Figure 13). Therefore, it is concluded that the stronger Y 3d doublet ($3d_{3/2}$ and $3d_{5/2}$ peaks at *ca.* 161 and 159 eV, respectively) is due to yttrium ions on the surface and the weaker Y 3d doublet ($3d_{3/2}$ and $3d_{5/2}$ peaks at *ca.* 159 and 157 eV, respectively) is due to yttrium ions inside the crystal.

The XPS spectra show also a singlet peak due to the Na 1s electrons at ca. 1072 eV with all the $NaYF_4$:Yb^{3+},Tb^{3+} materials before and after the sputtering (Figure 21).[161] The only notable difference is the weaker intensity of the as-prepared materials as it is with the Y 3d peaks (Figure 20). Since only one singlet peak is obtained, all the Na ions have a very similar chemical environment. Earlier it was suspected that the layer covering the particles (Figure 13) could be due to NaF but these results seems to be against that theory since there is only one singlet due to sodium (Figure 21). However, this is not certain because there might be two overlapping singlets. Also the Na 1s binding energies are higher with water washings – as it is with the Y 3d peaks.

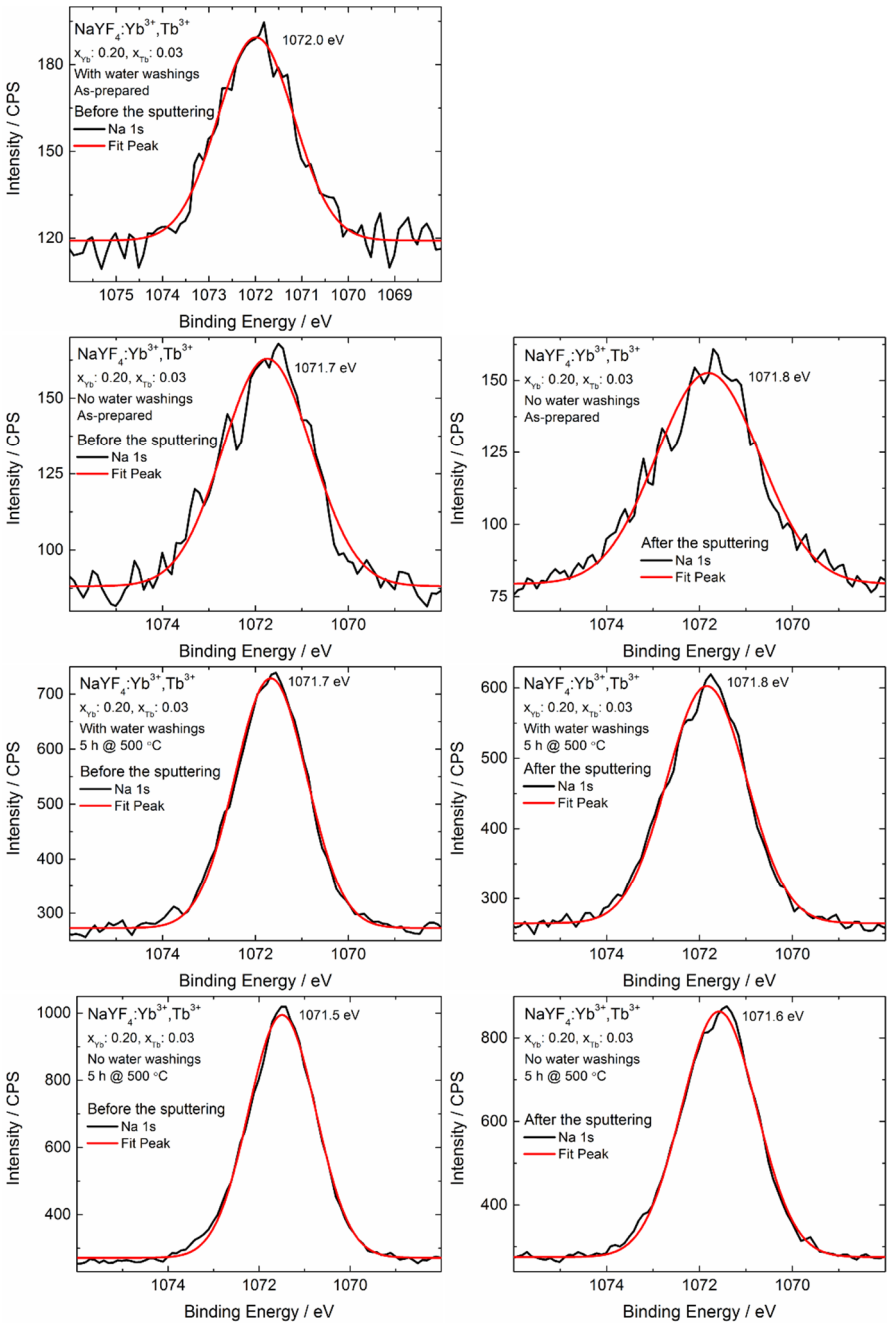

Figure 21. Na (1s) XPS spectra with fitting curves of the as-prepared and annealed $NaYF_4:Yb^{3+},Tb^{3+}$ materials obtained with and without the water washings before (left) and after (right) the sputtering.

All the $NaYF_4$:Yb^{3+},Tb^{3+} materials show also a singlet peak due to the F 1s electrons at *ca.* 685 eV and again the as-prepared materials have weaker intensity (Figure 22). However, a second singlet is obtained at slightly higher binding energy with the material without the water washings. Therefore, there is fluoride ions with two different chemical environments. The stronger singlet at *ca.* 685 eV is probably due to the fluoride ions on the surface and the weaker singlet at *ca.* 686 eV is due to fluoride ions inside the crystal. The presence of the two singlets could be due to the layer covering the particles (Figure 13 a and c). Thus, these results support the NaF layer hypothesis unlike the sodium peaks (Figure 21). It is interesting to see that also the F 1s peaks, as well as the Y 3d and Na 1s, have higher binding energies with the water washings. However, the reason is yet unclear.

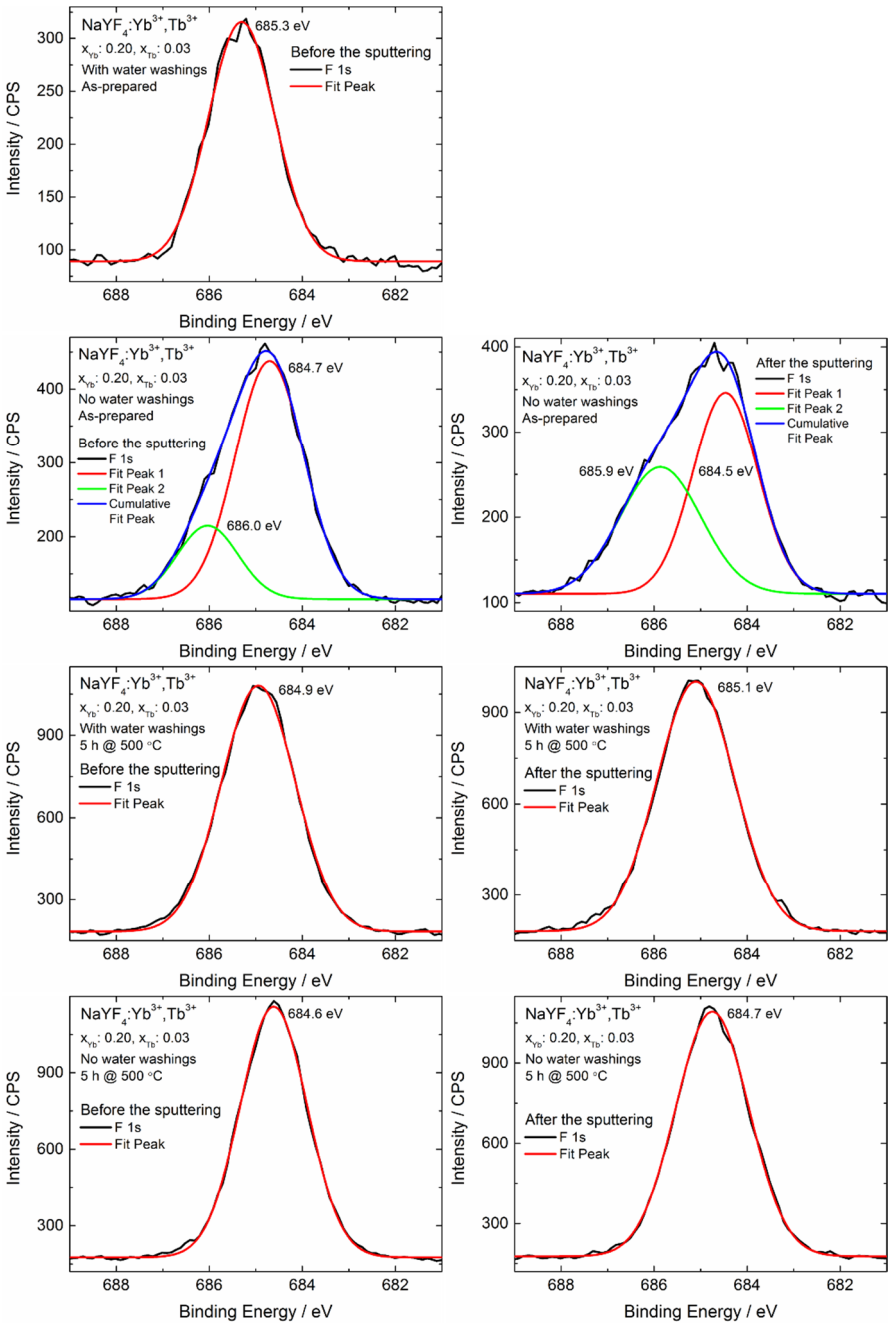

Figure 22. F (1s) XPS peaks with fitting curves of the as-prepared and annealed $NaYF_4:Yb^{3+},Tb^{3+}$ materials prepared with and without the water washings before (left) and after (right) the sputtering.

5.1.7. *Up-conversion Luminescence Enhancement*

The most important consequence of omitting the water washings is that the up-conversion luminescence of the $NaYF_4:Yb^{3+},Tb^{3+}$ material is 1-2 orders of magnitude stronger (Figure 23; I-III) – even though both washing methods resulted in the hexagonal structure. The up-conversion luminescence is not only stronger in general but also some new emissions, such as the Tb^{3+} $^5D_3 \rightarrow {}^7F_{6\text{-}2}$, are now visible.

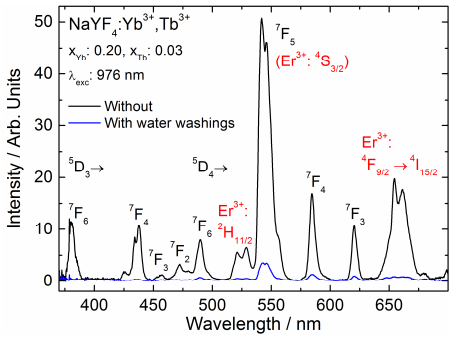

Figure 23. Up-conversion luminescence spectra of the hexagonal $NaYF_4:Yb^{3+},Tb^{3+}$ materials prepared with and without the water washings.

The structural details, affecting the up-conversion luminescence enhancement of the $NaYF_4:Yb^{3+},Tb^{3+}$, were studied with the Williamson-Hall and Rietveld analyses of the XPD data (I). First of all, as mentioned earlier, the crystal form is the hexagonal with both washing methods. Moreover, the only impurity obtained is NaF with the material without the water washings.

The Williamson-Hall analyses indicate only slightly larger crystallite size (110 and 94 nm) for the high intensity material prepared without the water washings. Therefore, the size is not at least the main reason causing the luminescent enhancement. The ε value, on the other hand, is 0.04 and 0.008 % with and without the water washings, respectively. This means the material without the water washings has less microstrains which can quench luminescence by causing energy traps and non-radiative relaxation processes. The smaller amount of strains is a

consequence from the *ca.* 100 °C lower cubic-to-hexagonal phase transition temperature (III) giving more time to relax the structural strains resulting from the phase transition (I).

The Rietveld analyses show very similar results with both washing methods (I). Nevertheless, the material without the water washings has a tiny deficit of Y^{3+} and Ln^{3+} (Na/(Y+Ln) ratio is 101 %) which may increase the up-conversion luminescence by limiting excess energy migration in the Yb sublattice. Also these studies suggest that there might be cation re-ordering (involving Y^{3+} and Ln^{3+} ions occupying the Na site) with the material without the water washings which would enhance the Yb^{3+}-Tb^{3+} energy transfer and thus enhance the luminescence. This was later studied with EXAFS (II).

EXAFS was used to calculate the distance distributions around Y^{3+}, Yb^{3+} and Tb^{3+} (II). The Tb-F distance is the same (0.234 nm) with both washing methods. The Y-F and Yb-F distances are slightly different with the material with the water washings while the distances are the same (0.230 nm) with the material without the water washings. This suggest the latter material have fewer distortions in the Y/Ln sublattice which supports the Williamson-Hall microstrain analysis (I).

Moreover, without the water washings the signal around 0.32-0.40 nm is stronger than with the water washings suggesting that there is an increased number of Yb^{3+} ions occupying the Na sites and that these Yb species have formed clusters with the Tb^{3+} occupying the regular Na/Y/Ln sites (II). This improves the Yb^{3+}-Tb^{3+} energy transfer resulting in up-conversion luminescence enhancement. Together with the Rietveld analyses (I) it was found out that as much as 10 mol-% (*ca.* 2 % of the total cation amount) of the Yb^{3+} ions can occupy the Na site (II).

5.2. Effect of Erbium Impurity on the Up-conversion Luminescence of Terbium

The very good efficiency of the up-conversion luminescence of the Yb^{3+},Er^{3+} pair, the presence of Er^{3+} as an impurity in the yttrium and

lanthanide oxide precursors and the weakness of the Tb^{3+} up-conversion luminescence gave us a reason to suspect that Er^{3+} might have a role in the up-conversion luminescence mechanism of Tb^{3+} (III). Up-conversion luminescence of Er^{3+} (and Tm^{3+} as well) is obtained even from $NaYF_4$ and $NaYbF_4$ materials (Figure 24) without intentional Er^{3+} doping – when the impurity Er^{3+} concentration is probably on the scale of couple hundred ppm (parts per million) at the most.

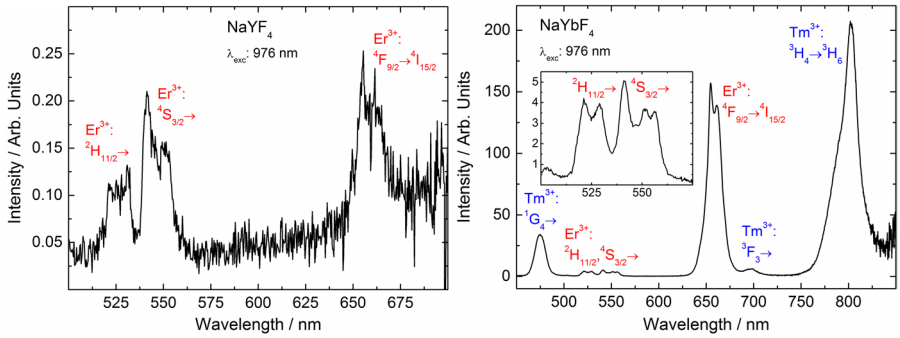

Figure 24. Up-conversion luminescence spectra of the $NaYF_4$ and $NaYbF_4$ materials.

The $NaYF_4$:Yb^{3+} material shows strong up-conversion luminescence of the Er^{3+} and Tm^{3+} impurities (Figure 25). However, the intensities of these emissions decrease strongly when Tb^{3+} is added as a co-dopant, continue decreasing by increasing Tb^{3+} concentration and vanish completely when the Tb^{3+} concentration is *ca.* 7-8 mol-%. At the same time, the intensity of the Tb^{3+} up-conversion luminescence enhances and is the strongest with 6 mol-% Tb^{3+} after which the $^5D_3 \rightarrow {}^7F_{6\text{-}2}$ emissions weaken due to the $(^5D_3, {}^7F_6) \rightarrow (^5D_4, {}^7F_1)$ cross-relaxation mechanism.

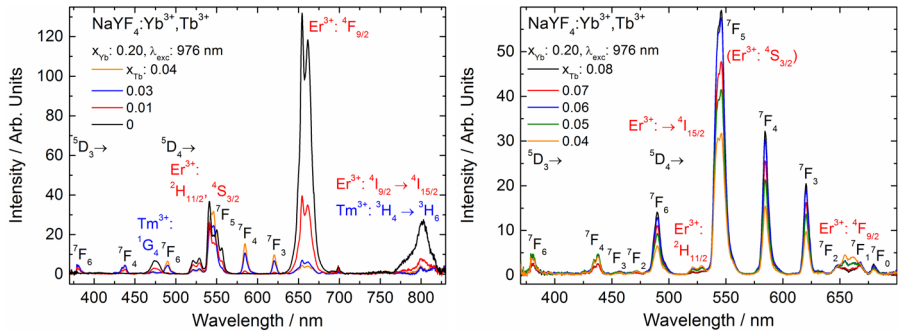

Figure 25. Up-conversion luminescence spectra of the $NaYF_4:Yb^{3+}$ and $NaYF_4:Yb^{3+},Tb^{3+}$ (x_{Tb}: 0.01-0.08) materials.

As the emissions from the Er^{3+} and Tm^{3+} impurities weaken and finally vanish with increasing Tb^{3+} concentration, up-conversion luminescence rise and decay times of the 544 nm emission increase (Figure 26). The rise and decay times increase until the Tb^{3+} concentration reaches 3 mol-% after which those are quite similar with all the dopant concentrations (x_{Tb}: 0.03-0.08). The up-conversion emission rise time increases from *ca.* 2 ms without Tb^{3+} to *ca.* 8 ms with 3-8 mol-% Tb^{3+}. Moreover, the shape of the rise curve is quite different with the intermediate 3 and 4 mol-% Tb^{3+} concentrations compared to the higher concentrations even though the highest intensity is reached in about the same time (Figure 26 left).

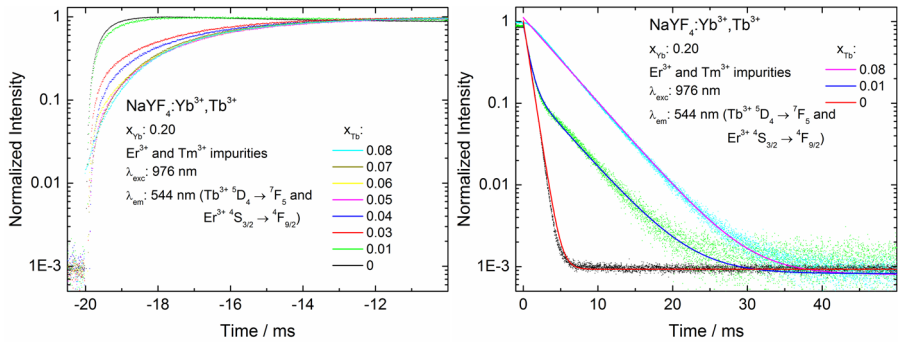

Figure 26. Up-conversion luminescence rise (left) and decay (right) curves of the $NaYF_4:Yb^{3+}$ and selected $NaYF_4:Yb^{3+},Tb^{3+}$ materials measured at 544 nm after 976 nm excitation.

The lifetime of the 544 nm emission increases from *ca.* 0.7 ms without the Tb^{3+} co-doping to *ca.* 4.1-4.2 ms with 3-8 mol-% Tb^{3+} (Table 6). Two different lifetimes (*ca.* 0.7 and 4.2 ms) are observed with 1 mol-% Tb^{3+}. With the $NaYF_4$:Yb^{3+} material the emission at 544 nm is only from the Er^{3+} impurity due to the $^4S_{3/2} \rightarrow {}^4F_{9/2}$ transition and with the Tb^{3+} co-doping also due to the $^5D_4 \rightarrow {}^7F_5$ transition – at least with 1 mol-% Tb^{3+} showing two different lifetimes. Also the decay curve with 1 mol-% seems to have two different parts: first the intensity decreases rapidly like without Tb^{3+} (only Er^{3+} emission present) and then the intensity decreases slower like with 8 mol-% Tb^{3+} (Figure 25 right). In other words, Er^{3+} and Tb^{3+} emissions are overlapping around 544 nm (Figure 25). Therefore, the shorter *ca.* 0.7 ms lifetime is due to Er^{3+} and the longer *ca.* 4.1-4.2 ms lifetime is due to Tb^{3+}. All in all, it is concluded that all these observations (Figures 24-26) supports the hypothesis of Er^{3+} having a role on the up-conversion luminescence mechanism of Tb^{3+} by Yb^{3+}-Er^{3+}-Tb^{3+} energy transfer.

Table 6. Up-conversion luminescence lifetimes (t) of the $NaYF_4$:Yb^{3+} and $NaYF_4$:Yb^{3+},Tb^{3+} (x_{Tb}: 0.01-0.08) materials measured at 544 nm after 976 nm excitation.

x_{Tb}	t_1 / ms	t_2 / ms	x_{Tb}	t_1 / ms	t_2 / ms
0.08	4.2	-	0.04	4.1	-
0.07	4.1	-	0.03	4.2	-
0.06	4.1	-	0.01	0.7	4.2
0.05	4.2	-	0	0.7	-

It was interesting to observe how the decay curves measured for the 488 nm emission of Tb^{3+} (Figure 27), without any contribution from Er^{3+}, show a very similar behaviour than the ones measured of the 544 nm emission (Figure 26). The difference in the shape of the rise part is not that big but with 0 and 1 mol-% Tb^{3+} the maximum intensity is reached a little faster than with the higher Tb^{3+} concentrations: *ca.* 6 vs. 8 ms. Also the decay part shows smaller differences but they are clear

anyway: without Tb^{3+} the intensity decreases faster than with 3-8 mol-% Tb^{3+} and the material with 1 mol-% Tb^{3+} show both the fast and slow parts.

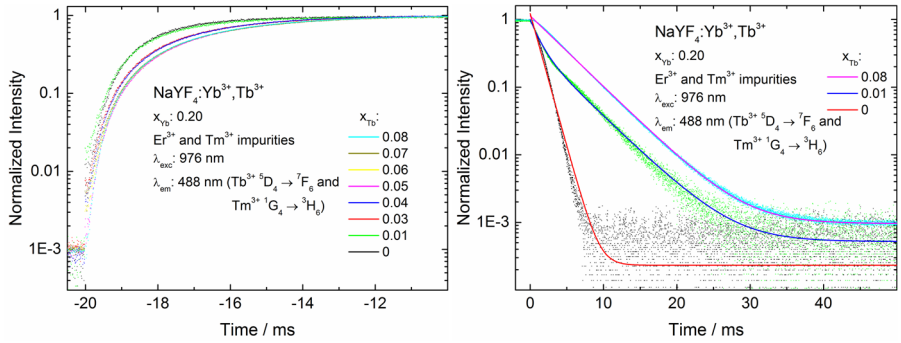

Figure 27. Up-conversion luminescence excitation (left) and decay (right) curves of the $NaYF_4:Yb^{3+}$ and selected $NaYF_4:Yb^{3+},Tb^{3+}$ materials measured at 488 nm after 976 nm excitation.

The fact that the emission at 488 nm is observed even without the Tb^{3+} doping is due to the presence of the Tm^{3+} impurity. This is because the bandpass filter used to select the measured emission lets trough also some of the Tm^{3+} $^1G_4 \rightarrow {}^3H_6$ emission centered at 475 nm (Figure 25). The lifetimes of the Tm^{3+} $^1G_4 \rightarrow {}^3H_6$ and Tb^{3+} $^5D_4 \rightarrow {}^7F_6$ emissions are *ca.* 1.1 and 4.1 ms, respectively (Table 7). Finally, these results suggest that also Tm^{3+} might have a role on the up-conversion luminescence mechanism of Tb^{3+} by the Yb^{3+}-Tm^{3+}-Tb^{3+} energy transfer.

Table 7. Up-conversion luminescence lifetimes (t) of the $NaYF_4:Yb^{3+}$ and $NaYF_4:Yb^{3+},Tb^{3+}$ (x_{Tb}: 0.01-0.08) materials measured at 488 nm after 976 nm excitation.

x_{Tb}	t_1 / ms	t_2 / ms	x_{Tb}	t_1 / ms	t_2 / ms
0.08	4.2	-	0.04	4.2	-
0.07	4.1	-	0.03	4.1	-
0.06	4.0	-	0.01	1.2	4.2
0.05	4.2	-	0	1.1	-

5.3. Estimating the Amount of the Impurity Cubic Form

The cubic form was obtained as an impurity with some materials, depending on the dopant and its concentration, when the water washing method was used (V). One of the most interesting things was to observe the relation between the amount of the impurity cubic form and the specific enthalpy of the cubic-to-hexagonal phase transition. The cubic-to-hexagonal phase transitions tends to occur at higher temperature with more cubic form present after the annealing. Moreover, the exothermic DSC signal, showing the cubic-to-hexagonal transition, weakens at the same time (V). So far there has not been any trace of the cubic form if the specific enthalpy is over 65 Jg^{-1}. The DSC measurements can now be used to estimate if there is going to be impurity cubic form present after the post-annealing. Since the DSC is faster than the post-annealing, this can save time and resources when developing new materials

5.4. Up-conversion Luminescence of Other Lanthanides

The optimized synthesis conditions discussed above (section 5.1.7) were used to prepare other hexagonal $NaYF_4:Yb^{3+},Ln^{3+}$ materials to obtain a wider selection of up-conversion luminescence. Because of the enhanced emission intensities obtained, strong up-conversion luminescence was observed from activators that previously showed practically no emission (VI). Up-conversion luminescence is now observed from $NaYF_4:Yb^{3+}$ co-doped with Pr^{3+}, Nd^{3+}, Eu^{3+}, Tb^{3+}, Ho^{3+}, Er^{3+} or Tm^{3+} under 976 nm

excitation. Tm^{3+}, Er^{3+} and Ho^{3+} give clearly the strongest intensity while the rest are *ca.* 3-4 orders of magnitude weaker. Unfortunately, Sm^{3+} and Dy^{3+} still do not show any up-conversion luminescence in the $NaYF_4$ host under 976 nm excitation.

Sm^{3+} in the $^6H_{5/2}$ ground level does not have a transition in good resonance with the energies of the Yb^{3+} $^2F_{5/2} \rightarrow {}^2F_{7/2}$ transition or 976 nm laser (Figure 28).[26,91] However, the energies of the Sm^{3+} $^6H_{5/2} \rightarrow {}^6F_{11/2,9/2}$ transitions are very close which should enable phonon-assisted Yb^{3+}-Sm^{3+} energy transfer. Therefore, the absence of the Sm^{3+} up-conversion luminescence is probably due to the small energy differences between the $^6F_{1/2\text{-}11/2}$ and $^6H_{5/2\text{-}15/2}$ levels (*ca.* 700-1200 cm^{-1} max[26,91]) enabling efficient multiphonon de-excitation.

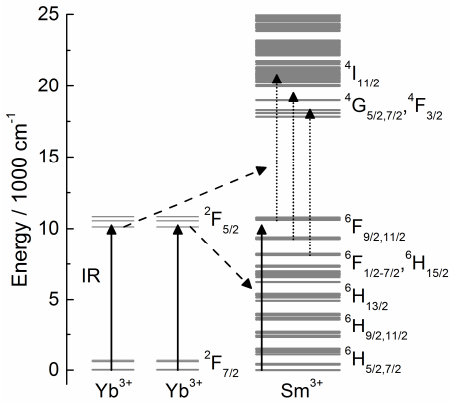

Figure 28. Up-conversion luminescence scheme of Yb^{3+} sensitized Sm^{3+} through 4f energy levels.[26,91]

The small differences between the energy levels of Sm^{3+} (Figure 28) will also enable many cross-relaxation processes which hinder up-conversion mechanism. Thus it is probable that Sm^{3+} will de-excite before it can absorb a second photon, which would subsequently excite Sm^{3+} to higher energy levels capable of emitting visible photons. It is even possible that Sm^{3+} quenches the very efficient Er^{3+} up-conversion luminescence because the emissions of the Er^{3+} impurity are not observed (VI).

Dy^{3+} in the $^6H_{15/2}$ ground level does have transitions in good resonance with the energies of the Yb^{3+} $^2F_{5/2} \rightarrow {}^2F_{7/2}$ transition and the 976 nm laser (Figure 29).[26,91] However, up-conversion to the higher energy levels which possibly emit visible photons (*e.g.* $^4F_{9/2}$) is possible only if the intermediate excited level is $^6F_{9/2}$ or higher ($^6F_{1/2\text{-}7/2}$). Even though Dy^{3+} would excite to these intermediate $^6F_{1/2\text{-}9/2}$ levels, which is improbable (at least inefficient) because the energies needed are higher than the excitation energy, it can de-excite due to multiphonon de-excitation because the energy differences between the $^6F_{1/2\text{-}9/2}$ and $^6H_{5/2,7/2}$ levels are small (*ca.* 1300 cm^{-1} max[26,91]). Cross-relaxation mechanisms are also efficient due to the large amount of energy levels between the $^6F_{1/2}$ and $^6H_{15/2}$ levels. As Sm^{3+}, Dy^{3+} might even quench the very efficient Er^{3+} up-conversion luminescence because the emissions of the Er^{3+} impurity are not observed with Dy^{3+} present (VI).

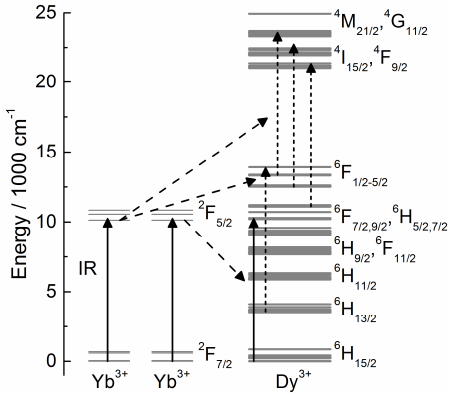

Figure 29. Up-conversion luminescence scheme of Yb^{3+} sensitized Dy^{3+} through 4f energy levels.[26,91]

Although Sm^{3+} and Dy^{3+} do not show any up-conversion luminescence, it is now possible to use only one synthesis method to produce several different up-conversion luminescence materials with the same host (VI). This can save lot of time and resources by requiring knowledge of only one synthesis and material type. Since each lanthanide has its characteristic multiple emissions, these materials show up-

conversion luminescence at the UV, violet, blue, green, yellow, orange, red and NIR wavelength ranges thus including almost the whole visible range. Moreover, additional color tuning is possible for example by changing the dopant concentrations and/or doping more than one activator in the same material. For example the Er^{3+} doped material has the CIE (Commission internationale de l'éclairage) color coordinate in the red region while the CIE color coordinate of Pr^{3+} doped material with some amount of Er^{3+} impurity is close to white (IV). This is again a good example of how impurities might affect the materials' properties and one should always keep in mind that there are, for sure, always some impurities in each material – detectable or not.

6. SUMMARY

Up-conversion luminescence is a unique phenomenon where lower energy radiation is converted to higher energy radiation: usually IR to visible. This is possible due to energy levels with long enough lifetimes to absorb and stack at least two photons before a radiative emission. Also ladder-like energy levels with matching energy differences are needed to enable efficient energy absorption, transfer and stacking.

Several lanthanides, such as Er^{3+}, Tm^{3+} and Ho^{3+}, fulfill these requirements very well and can act as an activator in these kind of materials. Depending on the energy level structure and excitation energy, an activator can excite through different up-conversion mechanisms of which ETU mechanism is the most efficient one. It includes an Yb^{3+} sensitizer which enhances the up-conversion by improving the energy absorption efficiency. However, the up-conversion quantum efficiency is still quite poor and an improvement is desired.

A host is needed because the activator concentration must be in the range of a couple percent to avoid cross-relaxation processes which quench the luminescence efficiency and $NaYF_4$ is among the best ones. It has low phonon energy which hinders the harmful multiphonon de-excitation processes and it is easy to prepare in different sizes and shapes with different dopants.

Lanthanide doped (Pr, Nd, Sm, Eu, Tb, Dy, Ho, Er, Tm and Yb) $NaYF_4$ materials were prepared with the co-precipitation synthesis to study up-conversion luminescence. Luminescence efficiency was improved by modifying the synthesis and structural properties were studied using TG-DSC, XPD, TEM, TOF-SIMS, XPS and EXAFS. As a result, a comprehensive selection of up-conversion luminescence materials, with wide selection of spectra and colors, is now available by mastering only one synthesis.

Now lanthanide doped $NaYF_4$ materials can be prepared always with the hexagonal crystal form which is better for the luminescence. Before also the cubic form was obtained with some materials and it was found out that the specific enthalpy of the cubic-to-hexagonal phase transition can help to predict the completeness of the phase transition: the probability of the cubic form being present increases with decreasing specific enthalpy.

The materials prepared with different synthesis conditions showed many differences in the properties between the old and the new improved material. The cubic-to-hexagonal phase transition occurs now at a 100 °C lower temperature and the crystal structure is always hexagonal. Unfortunately, the crystallites are now more aggregated resulting in a bigger particle size which could explain the stronger luminescence at least partly. However, the Williamson-Hall analyses indicated only a slightly larger crystallite size for the more luminescent samples suggesting that the size is not the main reason causing the luminescence enhancement.

The new materials are covered with a sodium-rich surface layer which might protect the lanthanides from the surface impurities decreasing the luminescence intensity. This might be at least one of the reasons why the up-conversion luminescence is now stronger. Anyway, it is known that the excess sodium is needed to form well crystallized hexagonal $NaYF_4:Yb^{3+},Ln^{3+}$ materials and these results confirm that when there is more sodium available the high intensity material is obtained. The presence of enough Na decreases the lattice strains and improves the energy transfer which results in stronger up-conversion luminescence.

In the future, the lanthanide doped $NaYF_4$ up-conversion luminescence materials would benefit from a better efficiency and the means for obtaining that should be studied further. The core-shell concept and addition of transition metals or organic compounds to enhance the energy absorption efficiency seem to be promising ways to proceed.

REFERENCES

1. Auzel, F. Upconversion and anti-Stokes processes with f and d ions in solids. *Chem. Rev.* **104,** 139–173 (2004).

2. Wang, F. & Liu, X. Recent advances in the chemistry of lanthanide-doped upconversion nanocrystals. *Chem. Soc. Rev.* **38,** 976–989 (2009).

3. Haase, M. & Schäfer, H. Upconverting nanoparticles. *Angew. Chem. Int. Ed. Engl.* **50,** 5808–5829 (2011).

4. Grubb, S. G., Bennett, K. W., Cannon, R. S. & Humer, W. F. CW room-temperature blue upconversion fibre laser. *Electron. Lett.* **28,** 1243–1244 (1992).

5. Joubert, M. F., Guy, S. & Jacquier, B. Model of the photon-avalanche effect. *Phys. Rev. B* **48,** 10031–10037 (1993).

6. Scheps, R. Upconversion laser processes. *Prog. Quantum Electron.* **20,** 271–358 (1996).

7. Downing, E., Hesselink, L., Ralston, J. & Macfarlane, R. A three-color, solid-state, three-dimensional display. *Science* **273,** 1185–1189 (1996).

8. Gutmann, R., Ahlers, B., Kapkke, F., Paugstadt, R. & Franz-Burgholz, A. Security document with optically excitable dyes for authenticity check. US Patent 6,234,537 (2001).

9. Shalav, A., Richards, B. S., Trupke, T., Krämer, K. W. & Güdel, H. U. Application of $NaYF_4:Er^{3+}$ up-converting phosphors for enhanced near-infrared silicon solar cell response. *Appl. Phys. Lett.* **86,** 13505 (2005).

10. de Wild, J., Meijerink, A., Rath, J. K., van Sark, W. G. J. H. M. & Schropp, R. E. I. Upconverter solar cells: materials and applications. *Energy Environ. Sci.* **4,** 4835–4848 (2011).

11. Zou, W., Visser, C., Maduro, J. A., Pshenichnikov, M. S. & Hummelen, J. C. Broadband dye-sensitized upconversion of near-infrared light. *Nat. Photonics* **6,** 560–564 (2012).

12. Huang, X., Han, S., Huang, W. & Liu, X. Enhancing solar cell efficiency: the search for luminescent materials as spectral converters. *Chem. Soc. Rev.* **42,** 173–201 (2013).

13. Fischer, S., Fröhlich, B., Steinkemper, H., Krämer, K. W. & Goldschmidt, J. C. Absolute upconversion quantum yield of β-$NaYF_4$ doped with Er^{3+} and external quantum efficiency of upconverter solar cell devices under broad-band excitation considering spectral mismatch corrections. *Sol. Energy Mater. Sol. Cells* **122,** 197–207 (2014).

14. Antal, T., Harju, E., Pihlgren, L., Lastusaari, M., Tyystjärvi, T., Hölsä, J. & Tyystjärvi, E. Use of near-infrared radiation for oxygenic photosynthesis via photon up-conversion. *Int. J. Hydrogen Energy* **37,** 8859–8863 (2012).

15. Nyk, M., Kumar, R., Ohulchanskyy, T. Y., Bergey, E. J. & Prasad, P. N. High contrast in vitro and in vivo photoluminescence bioimaging using near infrared to near infrared up-conversion in Tm^{3+} and Yb^{3+} doped fluoride nanophosphors. *Nano Lett.* **8,** 3834–3838 (2008).

16. Wang, M., Mi, C.-C., Wang, W.-X., Liu, C.-H., Wu, Y.-F., Xu, Z.-R., Mao, C.-B. & Xu, S.-K. Immunolabeling and NIR-excited fluorescent imaging of HeLa cells by using $NaYF_4$:Yb,Er upconversion nanoparticles. *ACS Nano* **3,** 1580–1586 (2009).

17. Yang, Y., Shao, Q., Deng, R., Wang, C., Teng, X., Cheng, K., Cheng, Z., Huang, L., Liu, Z., Liu, X. & Xing, B. In vitro and in vivo uncaging and bioluminescence imaging by using photocaged upconversion nanoparticles. *Angew. Chem. Int. Ed. Engl.* **51,** 3125–3129

(2012).

18. Zhou, J., Liu, Z. & Li, F. Upconversion nanophosphors for small-animal imaging. *Chem. Soc. Rev.* **41,** 1323–1349 (2012).

19. Tian, G., Gu, Z., Zhou, L., Yin, W., Liu, X., Yan, L., Jin, S., Ren, W., Xing, G., Li, S. & Zhao, Y. Mn^{2+} dopant-controlled synthesis of $NaYF_4$:Yb/Er upconversion nanoparticles for in vivo imaging and drug delivery. *Adv. Mater.* **24,** 1226–1231 (2012).

20. Ylihärsilä, M., Valta, T., Karp, M., Hattara, L., Harju, E., Hölsä, J., Saviranta, P., Waris, M. & Soukka, T. Oligonucleotide array-in-well platform for detection and genotyping human adenoviruses by utilizing upconverting phosphor label technology. *Anal. Chem.* **83,** 1456–1461 (2011).

21. Wu, S., Han, G., Milliron, D. J., Aloni, S., Altoe, V., Talapin, D. V, Cohen, B. E. & Schuck, P. J. Non-blinking and photostable upconverted luminescence from single lanthanide-doped nanocrystals. *Proc. Natl. Acad. Sci. U. S. A.* **106,** 10917–10921 (2009).

22. Zhang, C., Yuan, Y., Zhang, S., Wang, Y. & Liu, Z. Biosensing platform based on fluorescence resonance energy transfer from upconverting nanocrystals to graphene oxide. *Angew. Chem. Int. Ed. Engl.* **50,** 6851–6854 (2011).

23. Stepuk, A., Mohn, D., Grass, R. N., Zehnder, M., Krämer, K. W., Pellé, F., Ferrier, A. & Stark, W. J. Use of NIR light and upconversion phosphors in light-curable polymers. *Dent. Mater.* **28,** 304–311 (2012).

24. Yi, G., Lu, H., Zhao, S., Ge, Y., Yang, W., Chen, D. & Guo, L.-H. Synthesis, characterization, and biological application of size-controlled nanocrystalline $NaYF_4$:Yb,Er infrared-to-visible up-conversion phosphors. *Nano Lett.* **4,** 2191–2196 (2004).

25. van Dijk, J. M. F. & Schuurmans, M. F. H. On the nonradiative and radiative decay rates and a modified exponential energy gap law for 4f–4f transitions in rare-earth ions. *J. Chem. Phys.* **78,** 5317 (1983).

26. Kano, T. in *Phosphor Handbook* (eds. Yen, W. M., Shionoya, S. & Yamamoto, H.) 192–214 (CRC Press, 2006).

27. Carnall, W. T., Goodman, G. L., Rajnak, K. & Rana, R. S. A systematic analysis of the spectra of the lanthanides doped into single crystal LaF_3. *J. Chem. Phys.* **90,** 3443–3457 (1989).

28. Blasse, G. & Grabmaier, B. C. in *Luminescent Materials* 26 (Springer-Verlag, 1994).

29. de Sousa Filho, P. C., Lima, J. F. & Serra, O. A. From lighting to photoprotection: Fundamentals and applications of rare earth materials. *J. Braz. Chem. Soc.* **26,** 2471–2495 (2015).

30. Strohhöfer, C. & Polman, A. Absorption and emission spectroscopy in Er^{3+}-Yb^{3+} doped aluminum oxide waveguides. *Opt. Mater.* **21,** 705–712 (2003).

31. Kale, V., Lastusaari, M., Hölsä, J. & Soukka, T. Intense UV upconversion through highly sensitized $NaRF_4$:Tm (R:Y,Yb) crystals. *RSC Adv.* **5,** 35858–35865 (2015).

32. Dong, H., Sun, L.-D. & Yan, C.-H. Energy transfer in lanthanide upconversion studies for extended optical applications. *Chem. Soc. Rev.* **44,** 1608–1634 (2015).

33. Balda, R., Fernández, J., Mendioroz, A., Voda, M. & Al-Saleh, M. Infrared-to-visible upconversion processes in Pr^{3+}/Yb^{3+}-codoped KPb_2Cl_5. *Phys. Rev. B* **68,** 165101 (2003).

34. Naccache, R., Speghini, A., Bettinelli, M., Capobianco, J. A. & Vetrone, F. Cross-relaxation and upconversion processes in Pr^{3+} singly doped and Pr^{3+}/Yb^{3+} codoped nanocrystalline $Gd_3Ga_5O_{12}$: The sensitizer/activator relationship. *J. Phys. Chem. C* **112,** 7 (2008).

35. Hao, S., Shao, W., Qiu, H., Shang, Y., Fan, R., Guo, X., Zhao, L., Chen, G. & Yang, C. Tuning the size and upconversion emission of $NaYF_4$:Yb^{3+}/Pr^{3+} nanoparticles through Yb^{3+} doping. *RSC Adv.* **4,** 56302–56306 (2014).

36. Hirao, K., Higuchi, M. & Soga, N. Upconversion mechanism of Pr^{3+}-doped fluoride fiber glass. *J. Lumin.* **60–61,** 115–118 (1994).

37. Fernández, J., Balda, R., Mendioroz, A. & García-Adeva, A. J. Upconversion processes in Pr^{3+}-doped chalcohalide glasses. *J. Phys. Condens. Matter* **13,** 10347–10358 (2001).

38. Dereń, P. J., Mahiou, R., Strk, W., Bednarkiewicz, A. & Bertrand, G. Up-conversion in $KYb(WO_4)_2$:Pr^{3+} crystal. *Opt. Mater.* **19,** 145–148 (2002).

39. Gouveia-Neto, A. S., Da Costa, E. B., Bueno, L. A. & Ribeiro, S. J. L. Red, green, and blue upconversion luminescence in ytterbium-sensitized praseodymium-doped lead-cadmium-germanate glass. *Opt. Mater.* **26,** 271–274 (2004).

40. Velázquez, J. J., Yanes, A. C., Del-Castillo, J., Méndez-Ramos, J. & Rodríguez, V. D. Spectroscopic characterization and up-conversion in sol-gel derived Yb^{3+}-Pr^{3+} co-doped SiO_2-LaF_3 nano-glass-ceramics. *J. Non. Cryst. Solids* **356,** 1349–1353 (2010).

41. Holliday, K., Russell, D. L. & Henderson, B. Up-conversion spectroscopy of Nd^{3+}:$KLiYF_5$. *J. Lumin.* **72–74,** 927–929 (1997).

42. Zhang, X., Daran, E., Serrano, C. & Lahoz, F. Up-conversion fluorescence in MBE-grown Nd^{3+}-doped LaF_3/CaF_2 waveguides. *J. Lumin.* **87–89,** 1011–1013 (2000).

43. Fernández, J., Balda, R., Sanz, M., Lacha, L. M., Oleaga, A. & Adam, J. L. Upconversion losses in Nd-doped fluoroarsenate glasses. *J. Lumin.* **94–95,** 325–329 (2001).

44. Balda, R., Sanz, M., Mendioroz, A., Fernández, J., Griscom, L. & Adam, J.-L. Infrared-to-visible upconversion in Nd^{3+}-doped chalcohalide glasses. *Phys. Rev. B* **64,** 144101 (2001).

45. Fernández, J., Sanz, M., Mendioroz, A., Balda, R., Chaminade, J. P., Ravez, J., Lacha, L. M., Voda, M. & Arriandiaga, M. A. Site-selective spectroscopy and infrared-to-visible upconversion in a Nd^{3+}-doped $Pb_5Al_3F_{19}$ crystal. *J. Alloys Compd.* **323–324,** 267–272 (2001).

46. Wang, X., Song, J., Sun, H., Xu, Z. & Qiu, J. Multiphoton-excited upconversion luminescence of Nd:YVO_4. *Opt. Express* **15,** 1384 (2007).

47. Ramakrishna, P. V., Pammi, S. V. N. & Samatha, K. UV–visible upconversion studies of Nd^{3+} ions in lead tellurite glass. *Solid State Commun.* **155,** 21–24 (2013).

48. Zhou, Y., Lin, J. & Wang, S. Energy transfer and upconversion luminescence properties of Y_2O_3:Sm and Gd_2O_3:Sm phosphors. *J. Solid State Chem.* **171,** 391–395 (2003).

49. Som, T. & Karmakar, B. Infrared-to-red upconversion luminescence in samarium-doped antimony glasses. *J. Lumin.* **128,** 1989–1996 (2008).

50. Som, T. & Karmakar, B. Enhanced frequency upconversion of Sm^{3+} ions by elliptical Au nanoparticles in dichroic Sm^{3+}: Au-antimony glass nanocomposites. *Spectrochim. Acta - Part A Mol. Biomol. Spectrosc.* **75,** 640–646 (2010).

51. Wang, X., Yan, X. & Kan, C. Thermal loading induced near-infrared broadband upconversion emission of Sm^{3+}-doped β-$NaYbF_4$ nano-phosphors. *J. Lumin.* **131,** 2325–2329 (2011).

52. Wang, F., Deng, R., Wang, J., Wang, Q., Han, Y., Zhu, H., Chen, X. & Liu, X. Tuning upconversion through energy migration in core–shell nanoparticles. *Nat. Mater.* **10,** 968–973 (2011).

53. Strek, W., Dereń, P. J., Bednarkiewicz, A., Kalisky, Y. & Boulanger, P. Efficient up-conversion in $KYb_{0.8}Eu_{0.2}(WO_4)_2$ crystal. *J. Alloys Compd.* **300,** 180–183 (2000).

54. MacIel, G. S., Biswas, A. & Prasad, P. N. Infrared-to-visible Eu^{3+} energy upconversion due to cooperative energy transfer from an Yb^{3+} ion pair in a sol-gel processed multi-component silica glass. *Opt. Commun.* **178,** 65–69 (2000).

55. Dwivedi, Y., Thakur, S. N. & Rai, S. B. Study of frequency upconversion in Yb^{3+}/Eu^{3+} by cooperative energy transfer in oxyfluoroborate glass matrix. *Appl. Phys. B Lasers Opt.* **89,** 45–51 (2007).

56. Martín-Rodríguez, R., Valiente, R., Polizzi, S., Bettinelli, M., Speghini, A. & Piccinelli, F. Upconversion luminescence in nanocrystals of $Gd_3Ga_5O_{12}$ and $Y_3Al_5O_{12}$ doped with Tb^{3+}−Yb^{3+} and Eu^{3+}−Yb^{3+}. *J. Phys. Chem. C* **113,** 12195–12200 (2009).

57. Wang, L., Xue, X., Chen, H., Zhao, D. & Qin, W. Unusual radiative transitions of Eu^{3+} ions in Yb/Er/Eu tri-doped $NaYF_4$ nanocrystals under infrared excitation. *Chem. Phys. Lett.* **485,** 183–186 (2010).

58. Wang, L., Liu, Z., Chen, Z., Zhao, D., Qin, G. & Qin, W. Upconversion emissions from high-energy states of Eu^{3+} sensitized by Yb^{3+} and Ho^{3+} in β-$NaYF_4$ microcrystals under 980 nm excitation. *Opt. Express* **19,** 25471–25478 (2011).

59. Jiang, T., Liu, Y., Liu, S., Liu, N. & Qin, W. Upconversion emission enhancement of Gd^{3+} ions induced by surface plasmon field in Au@$NaYF_4$ nanostructures codoped with Gd^{3+}–Yb^{3+}–Tm^{3+} ions. *J. Colloid Interface Sci.* **377,** 81–87 (2012).

60. Stręk, W., Bednarkiewicz, A. & Dereń, P. J. Power dependence of luminescence of Tb^{3+}-doped $KYb(WO_4)_2$ crystal. *J. Lumin.* **92,** 229–235 (2001).

61. Salley, G. M., Valiente, R. & Guedel, H. U. Luminescence upconversion mechanisms in Yb^{3+}-Tb^{3+} systems. *J. Lumin.* **94–95,** 305–309 (2001).

62. Gouveia-Neto, A. S., Bueno, L. A., Afonso, A. C. M., Nascimento, J. F., Costa, E. B., Messaddeq, Y. & Ribeiro, S. J. L. Upconversion luminescence in Ho^{3+}/Yb^{3+}- and Tb^{3+}/Yb^{3+}-codoped fluorogermanate glass and glass ceramic. *J. Non. Cryst. Solids* **354,** 509–514 (2008).

63. Scarnera, V., Richards, B., Jha, A., Jose, G. & Stacey, C. Green up-conversion in Yb^{3+}-Tb^{3+} and Yb^{3+}-Tm^{3+}-Tb^{3+} doped fluoro-germanate bulk glass and fibre. *Opt. Mater.* **33,** 159–163 (2010).

64. Zhang, W. J., Chen, Q. J., Qian, Q., Zhang, Q. Y. & Jiang, Z. H. Cooperative energy transfer in Tb^{3+}/Yb^{3+}- and $Nd^{3+}/Yb^{3+}/Tb^{3+}$-codoped oxyfluoride glasses. *Phys. B Condens. Matter* **405,** 1062–1066 (2010).

65. Qiao, X., Fan, X., Xue, Z., Xu, X. & Luo, Q. Intense ultraviolet upconversion luminescence of Yb^{3+} and Tb^{3+} co-doped glass ceramics containing SrF_2 nanocrystals. *J. Lumin.* **131,** 2036–2041 (2011).

66. Qiao, X., Fan, X., Xue, Z., Xu, X. & Luo, Q. Upconversion luminescence of $Yb^{3+}/Tb^{3+}/Er^{3+}$-doped fluorosilicate glass ceramics containing SrF_2 nanocrystals. *J. Alloys Compd.* **509,** 4714–4721 (2011).

67. Prorok, K., Gnach, A., Bednarkiewicz, A. & Stręk, W. Energy up-conversion in Tb^{3+}/Yb^{3+} co-doped colloidal α-$NaYF_4$ nanocrystals. *J. Lumin.* **140,** 103–109 (2013).

68. Wermuth, M., Riedener, T. & Güdel, H. U. Spectroscopy and upconversion mechanisms of $CsCdBr_3$:Dy^{3+}. *Phys. Rev. B* **57,** 4369–4376 (1998).

69. Kam, C. H. & Buddhudu, S. NIR to visible upconversion emission from Dy^{3+}: ZBLYAN

glasses. *Solid State Commun.* **128,** 309–313 (2003).

70. Kumar Rai, V. & Rai, S. B. Optical transitions of Dy^{3+} in tellurite glass: Observation of upconversion. *Solid State Commun.* **132,** 647–652 (2004).

71. Tripathi, G., Rai, V. K. & Rai, S. B. Spectroscopy and upconversion of Dy^{3+} doped in sodium zinc phosphate glass. *Spectrochim. Acta - Part A Mol. Biomol. Spectrosc.* **62,** 1120–1124 (2005).

72. Rai, V. K., Rai, S. B. & Rai, D. K. Optical studies of Dy^{3+} doped tellurite glass: Observation of yellow-green upconversion. *Opt. Commun.* **257,** 112–119 (2006).

73. Li, A., Lü, Q., Zheng, Z., Sun, L., Wu, W., Liu, W., Yang, Y. & Lü, T. Yellow-green upconversion luminescence of Dy^{3+} ion in $LiNbO_3$ crystal heavily codoped with ZnO. *J. Appl. Phys.* **102,** 113102 (2007).

74. Dwivedi, Y. & Rai, S. B. Spectroscopic study of Dy^{3+} and Dy^{3+}/Yb^{3+} ions co-doped in barium fluoroborate glass. *Opt. Mater.* **31,** 1472–1477 (2009).

75. Li, C.-R., Li, S.-F., Dong, B., Sun, J.-C., Bo, X.-F. & Fan, X.-N. Intense up-conversion emissions of Yb^{3+}/Dy^{3+} co-doped Al_2O_3 nanopowders prepared by non-aqueous sol—gel method. *Chinese Phys. B* **21,** 97803 (2012).

76. Müller, P., Wermuth, M. & Güdel, H. U. Mechanisms of near-infrared to visible upconversion in $CsCdBr_3:Ho^{3+}$. *Chem. Phys. Lett.* **290,** 105–111 (1998).

77. Yi, G.-S. & Chow, G.-M. Colloidal LaF_3:Yb,Er, LaF_3:Yb,Ho and LaF_3:Yb,Tm nanocrystals with multicolor upconversion fluorescence. *J. Mater. Chem.* **15,** 4460 (2005).

78. Wang, X., Bu, Y., Xiao, S., Yang, X. & Ding, J. W. Upconversion in Ho^{3+}-doped YbF_3 particle prepared by coprecipitation method. *Appl. Phys. B Lasers Opt.* **93,** 801–807 (2008).

79. Xing, M., Cao, W., Zhong, H., Zhang, Y., Luo, X., Fu, Y., Feng, W., Pang, T. & Yang, X. Synthesis and upconversion luminescence properties of monodisperse Y_2O_3:Yb, Ho spherical particles. *J. Alloys Compd.* **509,** 5725–5730 (2011).

80. Zhang, H. X., Kam, C. H., Zhou, Y., Han, X. Q., Buddhudu, S. & Lam, Y. L. Visible up-conversion luminescence in $Er^{3+}:BaTiO_3$ nanocrystals. *Opt. Mater.* **15,** 47–50 (2000).

81. Suyver, J. F., Grimm, J., Krämer, K. W. & Güdel, H. U. Highly efficient near-infrared to visible up-conversion process in $NaYF_4:Er^{3+},Yb^{3+}$. *J. Lumin.* **114,** 53–59 (2005).

82. Mai, H., Zhang, Y., Sun, L.-D. & Yan, C.-H. Highly efficient multicolor up-conversion emissions and their mechanisms of monodisperse $NaYF_4$:Yb,Er core and core/shell-structured nanocrystals. *J. Phys. Chem. C* **111,** 13721–13729 (2007).

83. Hyppänen, I., Hölsä, J., Kankare, J., Lastusaari, M. & Pihlgren, L. Up-conversion luminescence properties of $Y_2O_2S:Yb^{3+},Er^{3+}$ nanophosphors. *Opt. Mater.* **31,** 1787–1790 (2009).

84. Heer, S., Kömpe, K., Güdel, H.-U. & Haase, M. Highly efficient multicolour upconversion emission in transparent colloids of lanthanide-doped $NaYF_4$ nanocrystals. *Adv. Mater.* **16,** 2102–2105 (2004).

85. Yin, A., Zhang, Y., Sun, L. & Yan, C. Colloidal synthesis and blue based multicolor upconversion emissions of size and composition controlled monodisperse hexagonal $NaYF_4$: Yb,Tm nanocrystals. *Nanoscale* **2,** 953–959 (2010).

86. Zeng, S., Ren, G., Li, W., Xu, C. & Yang, Q. Highly uniform Tm^{3+}-doped $NaYbF_4$ microtubes: Controlled synthesis and intense ultraviolet photoluminescence. *J. Phys. Chem. C* **114,** 10750–10754 (2010).

87. Liu, L., Li, B., Qin, R., Zhao, H., Ren, X. & Su,

Z. Synthesis and characterization of nanoporous $NaYF_4:Yb^{3+},Tm^{3+}@SiO_2$ nanocomposites. *Solid State Sci.* **12,** 345–349 (2010).

88. Xie, J., Zhang, Q., Zhuang, Y., Liu, X., Guan, M., Zhu, B., Yang, R. & Qiu, J. Enhanced mid-IR emission in Yb^{3+}-Tm^{3+} co-doped oxyfluoride glass ceramics. *J. Alloys Compd.* **509,** 3032–3037 (2011).

89. Nakazawa, E. & Shionoya, S. Cooperative luminescence in $YbPO_4$. *Phys. Rev. Lett.* **25,** 1710–1712 (1970).

90. Montoya, E., Espeso, O. & Bausá, L. E. Cooperative luminescence in Yb^{3+}:$LiNbO_3$. *J. Lumin.* **87,** 1036–1038 (2000).

91. Hölsä, J., Lastusaari, M., Maryško, M. & Tukia, M. A few remarks on the simulation and use of crystal field energy level schemes of the rare earth ions. *J. Solid State Chem.* **178,** 435–440 (2005).

92. Malta, O. L., Brito, H. F., Menezes, J. F. S., Silva, F. R. G. E., Donega, C. D. & Alves, S. Experimental and theoretical emission quantum yield in the compound Eu(thenoyltrifluoroacetonate)$_3$.2(dibenzyl sulfoxide). *Chem. Phys. Lett.* **282,** 233–238 (1998).

93. Lima, N. B. D., Gonçalves, S. M. C., Júnior, S. A. & Simas, A. M. A comprehensive strategy to boost the quantum yield of luminescence of europium complexes. *Sci. Rep.* **3,** 2395 (2013).

94. Boyer, J.-C. & van Veggel, F. C. J. M. Absolute quantum yield measurements of colloidal $NaYF_4$: Er^{3+}, Yb^{3+} upconverting nanoparticles. *Nanoscale* **2,** 1417–1419 (2010).

95. Zheng, W., Huang, P., Tu, D., Ma, E., Zhu, H. & Chen, X. Lanthanide-doped upconversion nano-bioprobes: electronic structures, optical properties, and biodetection. *Chem. Soc. Rev.* **44,** 1379–1415 (2015).

96. Goldschmidt, J. C. & Fischer, S. Upconversion for photovoltaics - a review of materials, devices and concepts for performance enhancement. *Adv. Opt. Mater.* **3,** 510–535 (2015).

97. Fischer, S., Johnson, N. J. J., Pichaandi, J., Goldschmidt, J. C. & van Veggel, F. C. J. M. Upconverting core-shell nanocrystals with high quantum yield under low irradiance: On the role of isotropic and thick shells. *J. Appl. Phys.* **118,** 193105 (2015).

98. Shao, W., Chen, G., Damasco, J., Wang, X., Kachynski, A., Ohulchanskyy, T. Y., Yang, C., Ågren, H. & Prasad, P. N. Enhanced upconversion emission in colloidal ($NaYF_4:Er^{3+}$)/$NaYF_4$ core/shell nanoparticles excited at 1523 nm. *Opt. Lett.* **39,** 1386–1389 (2014).

99. Chen, G., Ohulchanskyy, T. Y., Kachynski, A., Ågren, H. & Prasad, P. N. Intense visible and near-infrared upconversion photoluminescence in colloidal $LiYF_4:Er^{3+}$ nanocrystals under excitation at 1490 nm. *ACS Nano* **5,** 4981–4986 (2011).

100. Dyck, N. C., van Veggel, F. C. J. M. & Demopoulos, G. P. Size-dependent maximization of upconversion efficiency of citrate-stabilized β-phase $NaYF_4:Yb^{3+},Er^{3+}$ crystals via annealing. *ACS Appl. Mater. Interfaces* **5,** 11661–11667 (2013).

101. Xue, X., Uechi, S., Tiwari, R. N., Duan, Z., Liao, M., Yoshimura, M., Suzuki, T. & Ohishi, Y. Size-dependent upconversion luminescence and quenching mechanism of $LiYF_4$: Er^{3+}/Yb^{3+} nanocrystals with oleate ligand adsorbed. *Opt. Mater. Express* **3,** 989–999 (2013).

102. Faulkner, D. O., Petrov, S., Perovic, D. D., Kherani, N. P. & Ozin, G. A. Absolute quantum yields in $NaYF_4$:Er,Yb upconverters – synthesis temperature and power dependence. *J. Mater. Chem.* **22,** 24330–24334 (2012).

103. Chen, G., Shen, J., Ohulchanskyy, T. Y., Patel, N. J., Kutikov, A., Li, Z., Song, J., Pandey, R.

K., Ågren, H., Prasad, P. N. & Han, G. (α-$NaYbF_4$:Tm^{3+})/CaF_2 core/shell nanoparticles with efficient near-infrared to near-infrared upconversion for high-contrast deep tissue bioimaging. *ACS Nano* **6,** 8280–8287 (2012).

104. Xu, C. T., Svenmarker, P., Liu, H., Wu, X., Messing, M. E., Wallenberg, L. R. & Andersson-Engels, S. High-resolution fluorescence diffuse optical tomography developed with nonlinear upconverting nanoparticles. *ACS Nano* **6,** 4788–4795 (2012).

105. Fischer, S., Martín-Rodríguez, R., Fröhlich, B., Krämer, K. W., Meijerink, A. & Goldschmidt, J. C. Upconversion quantum yield of Er^{3+}-doped β-$NaYF_4$ and Gd_2O_2S: The effects of host lattice, Er^{3+} doping, and excitation spectrum bandwidth. *J. Lumin.* **153,** 281–287 (2014).

106. Kaivogen & Labrox. Upcon™. at http://www.upcon.fi/

107. de Mello, J. C., Wittmann, H. F. & Friend, R. H. An improved experimental determination of external photoluminescence quantum efficiency. *Adv. Mater.* **9,** 230–232 (1997).

108. Auzel, F. & Pecile, D. Absolute efficiency for IR to blue conversion materials and theoretical prediction for optimized matrices. *J. Lumin.* **11,** 321–330 (1976).

109. Würth, C., Geißler, D., Behnke, T., Kaiser, M. & Resch-Genger, U. Critical review of the determination of photoluminescence quantum yields of luminescent reporters. *Anal. Bioanal. Chem.* **407,** 59–78 (2015).

110. Thoma, R. E., Insley, H. & Hebert, G. M. The sodium fluoride-lanthanide trifluoride systems. *Inorg. Chem.* **5,** 1222–1229 (1966).

111. Harju, E., Hyppönen, I., Hölsä, J., Kankare, J., Lahtinen, M., Lastusaari, M., Pihlgren, L. & Soukka, T. Polymorphism of $NaYF_4$:Yb^{3+}, Er^{3+} up-conversion luminescence materials. *Zeitschrift für Krist. Proc.* **1,** 381–387 (2011).

112. PCPDFWIN v. 1.30, Powder diffraction file, 1997, international centre for diffraction data, entry 06-0342 (cubic $NaYF_4$).

113. PCPDFWIN v. 1.30, Powder diffraction file, 1997, international centre for diffraction data, entry 28-1192 (hexagonal $Na(Y_{0.57}Yb_{0.39}Er_{0.04})F_4$).

114. Schäfer, H., Ptacek, P., Eickmeier, H. & Haase, M. Synthesis of hexagonal Yb^{3+},Er^{3+}-doped $NaYF_4$ nanocrystals at low temperature. *Adv. Funct. Mater.* **19,** 3091–3097 (2009).

115. Krämer, K. W., Biner, D., Frei, G., Güdel, H. U., Hehlen, M. P. & Lüthi, S. R. Hexagonal sodium yttrium fluoride based green and blue emitting upconversion phosphors. *Chem. Mater.* **16,** 1244–1251 (2004).

116. Aebischer, A., Hostettler, M., Hauser, J., Krämer, K., Weber, T., Güdel, H. U. & Bürgi, H.-B. Structural and spectroscopic characterization of active sites in a family of light-emitting sodium lanthanide tetrafluorides. *Angew. Chem. Int. Ed. Engl.* **45,** 2802–2806 (2006).

117. Hyppänen, I., Hölsä, J., Kankare, J., Lastusaari, M., Pihlgren, L. & Soukka, T. Preparation and up-conversion luminescence properties of $NaYF_4$:Yb^{3+},Er^{3+} nanomaterials. *Terrae Rarae* 16:1-6 (2009).

118. Renero-Lecuna, C., Martín-Rodríguez, R., Valiente, R., González, J., Rodríguez, F., Krämer, K. W. & Güdel, H. U. Origin of the high upconversion green luminescence efficiency in β-$NaYF_4$:2%Er^{3+},20%Yb^{3+}. *Chem. Mater.* **23,** 3442–3448 (2011).

119. Suyver, J. F., Grimm, J., van Veen, M. K., Biner, D., Krämer, K. W. & Güdel, H. U. Upconversion spectroscopy and properties of $NaYF_4$ doped with Er^{3+}, Tm^{3+} and/or Yb^{3+}. *J. Lumin.* **117,** 1–12 (2006).

120. Lage, M. M., Moreira, R. L., Matinaga, F. M. & Gesland, J.-Y. Raman and infrared reflectivity

determination of phonon modes and crystal structure of Czochralski-grown $NaLnF_4$ (Ln = La, Ce, Pr, Sm, Eu, and Gd) single crystals. *Chem. Mater.* **17,** 4523–4529 (2005).

121. Shannon, R. D. Revised effective ionic radii and systematic studies of interatomic distances in halides and chalcogenides. *Acta Crystallogr. Sect. A* **32,** 751–767 (1976).

122. Mai, H.-X., Zhang, Y.-W., Si, R., Yan, Z.-G., Sun, L., You, L.-P. & Yan, C.-H. High-quality sodium rare-earth fluoride nanocrystals: Controlled synthesis and optical properties. *J. Am. Chem. Soc.* **128,** 6426–6436 (2006).

123. Chen, Z., Chen, H., Hu, H., Yu, M., Li, F., Zhang, Q., Zhou, Z., Yi, T. & Huang, C. Versatile synthesis strategy for carboxylic acid−functionalized upconverting nanophosphors as biological labels. *J. Am. Chem. Soc.* **130,** 3023–3029 (2008).

124. Zhang, Q. & Zhang, Q.-M. Synthesis and photoluminescent properties of α-$NaYF_4$:Nd/α-$NaYF_4$ core/shell nanostructure with enhanced near infrared (NIR) emission. *Mater. Lett.* **63,** 376–378 (2009).

125. Wang, M., Liu, J.-L., Zhang, Y.-X., Hou, W., Wu, X.-L. & Xu, S.-K. Two-phase solvothermal synthesis of rare-earth doped $NaYF_4$ upconversion fluorescent nanocrystals. *Mater. Lett.* **63,** 325–327 (2009).

126. Liang, X., Wang, X., Zhuang, J., Peng, Q. & Li, Y. Synthesis of $NaYF_4$ nanocrystals with predictable phase and shape. *Adv. Funct. Mater.* **17,** 2757–2765 (2007).

127. Wang, F., Han, Y., Lim, C. S., Lu, Y., Wang, J., Xu, J., Chen, H., Zhang, C., Hong, M. & Liu, X. Simultaneous phase and size control of upconversion nanocrystals through lanthanide doping. *Nature* **463,** 1061–1065 (2010).

128. Boyer, J.-C., Vetrone, F., Cuccia, L. A. & Capobianco, J. A. Synthesis of colloidal upconverting $NaYF_4$ nanocrystals doped with Er^{3+}, Yb^{3+} and Tm^{3+}, Yb^{3+} via thermal decomposition of lanthanide trifluoroacetate precursors. *J. Am. Chem. Soc.* **128,** 7444–7445 (2006).

129. Mai, H.-X., Zhang, Y.-W., Sun, L.-D. & Yan, C.-H. Size- and phase-controlled synthesis of monodisperse $NaYF_4$:Yb,Er nanocrystals from a unique delayed nucleation pathway monitored with upconversion spectroscopy. *J. Phys. Chem. C* **111,** 13730–13739 (2007).

130. Yi, G. S. & Chow, G. M. Synthesis of hexagonal-phase $NaYF_4$:Yb,Er and $NaYF_4$:Yb,Tm nanocrystals with efficient up-conversion fluorescence. *Adv. Funct. Mater.* **16,** 2324–2329 (2006).

131. Li, C., Yang, J., Quan, Z., Yang, P., Kong, D. & Lin, J. Different microstructures of β-$NaYF_4$ fabricated by hydrothermal process: Effects of pH values and fluoride sources. *Chem. Mater.* **19,** 4933–4942 (2007).

132. Wang, L. & Li, Y. $Na(Y_{1.5}Na_{0.5})F_6$ single-crystal nanorods as multicolor luminescent materials. *Nano Lett.* **6,** 1645–1649 (2006).

133. Wang, L. & Li, Y. Controlled synthesis and luminescence of lanthanide doped $NaYF_4$ nanocrystals. *Chem. Mater.* **19,** 727–734 (2007).

134. Li, C., Quan, Z., Yang, J., Yang, P. & Lin, J. Highly uniform and monodisperse β-$NaYF_4$:Ln^{3+} (Ln = Eu, Tb, Yb/Er, and Yb/Tm) hexagonal microprism crystals: Hydrothermal synthesis and luminescent properties. *Inorg. Chem.* **46,** 6329–6337 (2007).

135. Zeng, S., Yi, Z., Lu, W., Qian, C., Wang, H., Rao, L., Zeng, T., Liu, H., Liu, H., Fei, B. & Hao, J. Simultaneous realization of phase/size manipulation, upconversion luminescence enhancement, and blood vessel imaging in multifunctional nanoprobes through transition metal Mn^{2+} doping. *Adv. Funct. Mater.* **24,** 4051–4059 (2014).

136. Wang, F., Wang, J. & Liu, X. Direct evidence of

a surface quenching effect on size-dependent luminescence of upconversion nanoparticles. *Angew. Chemie - Int. Ed.* **49,** 7456–7460 (2010).

137. Naccache, R., Vetrone, F., Mahalingam, V., Cuccia, L. A. & Capobianco, J. A. Controlled synthesis and water dispersibility of hexagonal phase $NaGdF_4$:Ho^{3+}/Yb^{3+} nanoparticles. *Chem. Mater.* **21,** 717–723 (2009).

138. Boyer, J.-C., Manseau, M.-P., Murray, J. I. & van Veggel, F. C. J. M. Surface modification of upconverting $NaYF_4$ nanoparticles with PEG-phosphate ligands for NIR (800 nm) biolabeling within the biological window. *Langmuir* **26,** 1157–1164 (2010).

139. Yi, G. S. & Chow, G. M. Water-soluble $NaYF_4$:Yb,Er(Tm)/$NaYF_4$/polymer core/shell/shell nanoparticles with significant enhancement of upconversion fluorescence. *Chem. Mater.* **19,** 341–343 (2007).

140. Zhang, F., Che, R., Li, X., Yao, C., Yang, J., Shen, D., Hu, P., Li, W. & Zhao, D. Direct imaging the upconversion nanocrystal core/shell structure at the subnanometer level: Shell thickness dependence in upconverting optical properties. *Nano Lett.* **12,** 2852–2858 (2012).

141. Li, Z. & Zhang, Y. Monodisperse silica-coated polyvinyl-pyrrolidone/$NaYF_4$ nanocrystals with multicolor upconversion fluorescence emission. *Angew. Chemie - Int. Ed.* **45,** 7732–7735 (2006).

142. Ostrowski, A. D., Chan, E. M., Gargas, D. J., Katz, E. M., Han, G., Schuck, P. J., Milliron, D. J. & Cohen, B. E. Controlled synthesis and single-particle imaging of bright, sub-10 nm lanthanide-doped upconverting nanocrystals. *ACS Nano* **6,** 2686–2692 (2012).

143. Johnson, N. J. J., Korinek, A., Dong, C. & Van Veggel, F. C. J. M. Self-focusing by Ostwald ripening: A strategy for layer-by-layer epitaxial growth on upconverting nanocrystals. *J. Am. Chem. Soc.* **134,** 11068–11071 (2012).

144. Boyer, J.-C., Gagnon, J., Cuccia, L. A. & Capobianco, J. A. Synthesis, characterization, and spectroscopy of nanoparticles. *Communications* **19,** 3358–3360 (2007).

145. Li, Z., Zhang, Y. & Jiang, S. Multicolor core/shell-structured upconversion fluorescent nanoparticles. *Adv. Mater.* **20,** 4765–4769 (2008).

146. Liu, Y., Tu, D., Zhu, H., Li, R., Luo, W. & Chen, X. A strategy to achieve efficient dual-mode luminescence of Eu^{3+} in lanthanides doped multifunctional $NaGdF_4$ nanocrystals. *Adv. Mater.* **22,** 3266–3271 (2010).

147. Prorok, K., Pawlyta, M., Strek, W. & Bednarkiewicz, A. Energy migration up-conversion of Tb^{3+} in Yb^{3+} and Nd^{3+} co-doped active-core/active-shell colloidal nanoparticles. *Chem. Mater.* **28,** 2295–2300 (2016).

148. Vetrone, F., Naccache, R., Mahalingam, V., Morgan, C. G. & Capobianco, J. A. The active-core/active-shell approach: A strategy to enhance the upconversion luminescence in lanthanide-doped nanoparticles. *Adv. Funct. Mater.* **19,** 2924–2929 (2009).

149. Qian, H. S. & Zhang, Y. Synthesis of hexagonal-phase core-shell $NaYF_4$ nanocrystals with tunable upconversion fluorescence. *Langmuir* **24,** 12123–12125 (2008).

150. Scherrer, P. Bestimmung der Größe und der inneren Struktur von Kolloidteilchen mittels Röntgenstrahlen. *Nachrichten von der Gesellschaft der Wissenschaften zu Göttingen, Math. Klasse* **1918,** 98–100 (1918).

151. Patterson, A. L. The scherrer formula for X-ray particle size determination. *Phys. Rev.* **56,** 978–982 (1939).

152. Abel, K. A., Boyer, J. C. & Van Veggel, F. C. J. M. Hard proof of the $NaYF_4$/$NaGdF_4$ nanocrystal core/shell structure. *J. Am. Chem. Soc.* **131,** 14644–14645 (2009).

153. Abel, K. A., Boyer, J.-C., Andrei, C. M. & van

Veggel, F. C. J. M. Analysis of the shell thickness distribution on $NaYF_4$/$NaGdF_4$ core/shell nanocrystals by EELS and EDS. *J. Phys. Chem. Lett.* **2,** 185–189 (2011).

154. Rietveld, H. M. A profile refinement method for nuclear and magnetic structures. *J. Appl. Crystallogr.* **2,** 65–71 (1969).

155. Rodriguez-Carvajal, J. FullProf.2k. (2007).

156. Williamson, G. K. & Hall, W. H. X-ray line broadening from filed aluminium and wolfram. *Acta Metall.* **1,** 22–31 (1953).

157. Ungár, T. in *Industrial Applications of X-ray Diffraction* (eds. Chung, F. H. & Smith, D. K.) 847–852 (Marcel Dekker, 2000).

158. George, G. N. & Pickering, I. J. EXAFSPAK - a suite of computer programs for analysis of X-ray absorption spectra. (1993).

159. Origin 2015. (2015).

160. Mathews, M. D. D., Ambekar, B. R. R., Tyagi, A. K. K. & Köhler, J. High temperature X-ray diffraction studies on sodium yttrium fluoride. *J. Alloys Compd.* **377,** 162–166 (2004).

161. Moulder, J. F., Stickle, W. F., Sobol, P. E. & Bomben, K. D. *Handbook of X-ray photoelectron spectroscopy: A reference book of standard spectra for identification and interpretation of XPS Data.* (Physical Electronics, 1995).

162. Pichaandi, J., Das, G. K., Johnson, N. J. J., Regier, T. & van Veggel, F. C. J. M. Probing the structure of $NaYF_4$ nanocrystals using synchrotron-based energy-dependent X-ray photoelectron spectroscopy. *J. Phys. Chem. C* **118,** 21639–21646 (2014).